frontiers | Frontiers in Earth Science

TYPE Original Research
PUBLISHED 12 January 2023
DOI 10.3389/feart.2022.1077017

OPEN ACCESS

EDITED BY
Pingping Li,
China University of Petroleum, China

REVIEWED BY
Hengye Wei,
Southwest Petroleum University, China
Licheng Wang,
Institute of Tibetan Plateau Research (CAS), China

*CORRESPONDENCE
Shi Sun,
sstopwin@163.com
Anqing Chen,
aqinth@163.com

SPECIALTY SECTION
This article was submitted to Economic Geology,
a section of the journal
Frontiers in Earth Science

RECEIVED 22 October 2022
ACCEPTED 14 November 2022
PUBLISHED 12 January 2023

CITATION
Li R, Sun S, Xia W, Chen A, Ogg JG, Yang S, Xu S, Liao Z, Yang D and Hou M (2023), Late Guadalupian–early Lopingian marine geochemical records from the Upper Yangtze, South China: Implications for climate-biocrisis events.
Front. Earth Sci. 10:1077017.
doi: 10.3389/feart.2022.1077017

Late Guadalupian–early Lopingian marine geochemical records from the Upper Yangtze, South China: Implications for climate-biocrisis events

Ruixuan Li[1,2], Shi Sun[1,2]*, Wenpeng Xia[1,2], Anqing Chen[1,2]*, James G. Ogg[1,3], Shuai Yang[1], Shenglin Xu[1], Zhiwei Liao[4], Di Yang[2] and Mingcai Hou[1,2]

[1]Key Laboratory of Deep-Time Geography and Environment Reconstruction and Applications, MNR and Institute of Sedimentary Geology, Chengdu University of Technology, Chengdu, China, [2]State Key Laboratory of Oil and Gas Reservoir Geology and Exploitation, Chengdu University of Technology, Chengdu, China, [3]Department of Earth, Atmospheric and Planetary Sciences, Purdue University, West Lafayette, IN, United States, [4]School of Resources and Safety Engineering, State Key Laboratory of Coal Mine Disaster Dynamics and Control, Chongqing University, Chongqing, China

Major paleoenvironmental changes occurred during the Guadalupian-Lopingian boundary (GLB) transition, but the causative linkages among the Emeishan Large Igneous Province (LIP), end-Guadalupian crisis and climatic fluctuations are still in dispute. Variation of geochemical proxies preserved in the sedimentary records is important evidence in examining potential links between volcanisms and environmental changes. Herein, we carried out a comprehensive study of carbon/strontium isotope and trace element geochemistry at the Dukou section, northern margin of the Upper Yangtze. During the Late Guadalupian, the carbon isotope showed a negative drift, the marine primary productivity declined simultaneously, and redox proxies indicate the enhancement of ocean oxidation. It is worth noting that the $\delta^{13}C_{carb}$ turns into a rapid negative drift from a slow decline at approximately 260.55 Ma, which was almost synchronized with the latest reported eruption ages of Emeishan Large Igneous Province. This coincidence suggests that global volcanic-tectonic activity during the Late Guadalupian might have been the important factor in carbon-cycle perturbation. Subsequently, the $\delta^{13}C_{carb}$ presents a rapid positive shift at approximately 259.4 Ma, and climate transformed from interglacial to P4 glacial, indicating that the climate rapidly cooled before the Emeishan LIP completely ended, which may be due to carbon sinks caused by weathering of mafic rocks, and may also be associated with a significant reduction in global volcanic activity. Accompanied by sudden weathering attenuation, the $^{87}Sr/^{86}Sr$ ratios show a significant increase instead from the previous long-time low value, which only can be explained reasonably by the rapid decline in mantle-derived Sr flux associated with the weakening of volcanic activity and mafic weathering. Intergrated geochemical indices in this interval shows that there is a rapid climate perturbation associated with a significant $\delta^{13}C_{carb}$ negative shift at approximately 260.55 Ma ~ 259.10 Ma, which may be related to the eruption

surge of the Emeishan LIP, active volcanic arcs, and triggered the end-Guadalupian biocrisis.

KEYWORDS

geochemical proxies of carbonate, Emeishan LIP, end-Guadalupian transient warming event, Upper Yangtze, GLB transition

1 Introduction

The Guadalupian-Lopingian boundary (GLB) transition was a critical time interval during the Earth's evolution history, associated with global major changes of paleoclimate, paleo-ocean and paleogeography. Many special geological events occurred during this period, such as the onset of long-term ocean hypoxia (Isozaki, 1997; Wei et al., 2016; Zhang B. L. et al., 2021), a lowest sea-level in the Phanerozoic (Ross and Ross, 1987; Haq and Schutter, 2008; Chen et al., 2009), Emeishan Large Igneous Province (LIP) (Xu et al., 2010; Shellnutt, 2014; Zhong et al., 2014), initial breakup of Pangea (Maruyama et al., 2007; Isozaki, 2009; Santosh et al., 2009), Kamura event (Isozaki et al., 2007, 2011) and end-Guadalupian biocrisis (Stanley and Yang, 1994; Shen and Shi, 1996, 2002; Chen et al., 2009; Huang Y. G. et al., 2019), etc.

Accompanied by the violent eruption of the Emeishan LIP during the Late Guadalupian, which causing climatic fluctuations and ocean evolution (Chen et al., 2011; Zhang B. L. et al., 2021; Sun et al., 2022). Emeishan volcanism is also considered to be a potential kill mechanism of the end-Guadalupian biodiversity crisis (Wignall et al., 2009; Bond et al., 2010; Chen and Xu, 2019; Huang et al., 2022). Simultaneously, causal links between volcanic activity, biological crisis, climate change, and other geological events are still under discussion (Wignall et al., 2009; Bond et al., 2010; Cao et al., 2018; Chen and Xu, 2019; Zhang B. L. et al., 2021; Sun et al., 2022). Marine carbonate rocks usually have the original geochemical composition that can approximately represent the paleo-seawater, and record the paleoenvironmental information such as seawater temperature (Zhao et al., 2022), redox conditions (Wignall and Twitchett, 1996; Rimmer, 2004; Tribovillard et al., 2006; Scholz et al., 2011; Takahashi and AuthorAnonymous, 2014; Shembilu and Azmy, 2022) and primary productivity (Tribovillard et al., 2006; Schoepfer et al., 2015). Nevertheless, due to global extensive regression, most regions have transformed from marine strata to non-marine strata (Ross and Ross, 1987; Haq and Schutter, 2008; Shen et al., 2020). There are relatively continuous marine carbonate rocks deposited in the South China at low-latitude region, which provide an excellent material for the paleoenvironment research. Moreover, the abundant marine fossils can constrain the sedimentary time of the strata.

Geochemical indicators in carbonate rocks can usually be used to indicate paleoenvironmental change (Shen et al., 2014; Takahashi and AuthorAnonymous, 2014; Li et al., 2017; Chen et al., 2021). The carbon isotope excursion is closely related to the global carbon-cycle (Kump and Arthur, 1999). Positive drift of $\delta^{13}C$ is usually linked to the burial of organic carbon, while negative drift of $\delta^{13}C$ indicates the rapid injection of light carbon materials (Saltzman et al., 2000; Li D. D. et al., 2018). Carbon isotope has rapid responses to environmental changes caused by volcanic eruptions (Arthur et al., 1985; Wignall et al., 2009; Isson et al., 2019), and tend to be globally isochronous. For example, associated with the eruption of the Siberian LIP, the $\delta^{13}C$ showed a rapid negative drift near the PTB boundary (Huang, 1994; Korte and Kozur, 2010; Shen et al., 2013). The strontium isotopic composition of seawater is mainly driven by two different fluxes (Li and Elderfield, 2013; Peucker-Ehrenbrink and Fiske, 2019; McArthur et al., 2020): 1) the unradiogenic hydrothermal mantle-derived strontium flux. 2) The more radiogenic crustal-derived strontium. Marine carbonates can record the relative variation of mantle-derived Sr flux (provided by volcanic activity) and crust-derived Sr flux (provided by continental weathering) (Wang et al., 2018, 2021; Li et al., 2021).

Here, we present several geochemical proxy signatures (carbon and strontium isotopes, trace elements of carbonate rocks) of Dukou section, northern margin of the Upper Yangtze. To investigate the GLB marine succession, comparing with other reported paleoenvironmental indicators and contemporaneous geological events. This paper discusses the driving mechanism of climatic fluctuation and biological crisis during the GLB transition.

2 Geological setting

During the Guadalupian, South China was situated in the equator at low-latitude region, and surrounded by the Paleotethys (Scotese, 2016) (Figure 1). Marine carbonate rocks rich in biological fossils were deposited in most regions of South China, which are called Maokou Formation in the Upper Yangtze region. Affected by the Emeishan LIP and the Dongwu movement in the Late Guadalupian, a local deep-water trough was formed in the northern margin of the Upper Yangtze (Yang et al., 2021), and shelf facies were developed (Jin et al., 1998; Shen et al., 2013; Hou et al., 2020) (Figure 1B).

This investigated Dukou section (31°42′11″N, 108°18′35″E) is located in the Xuanhan City on the northern margin of the Upper Yangtze, structurally belongs to the intersection zone between the Daba Mountain NW-trending structural belt and the Huaying Mountain NE-trending structural belt. The Dukou section is one of the relatively complete exposed Permian successions of South China (Jin et al., 1998; Shen et al., 2013; Hou et al., 2020), and in ascending order, the Liangshan, Chihsia, Maokou, Wuchiaping, and Changxing formations are exposed along both sides of the Lishi river (Figure 1C).

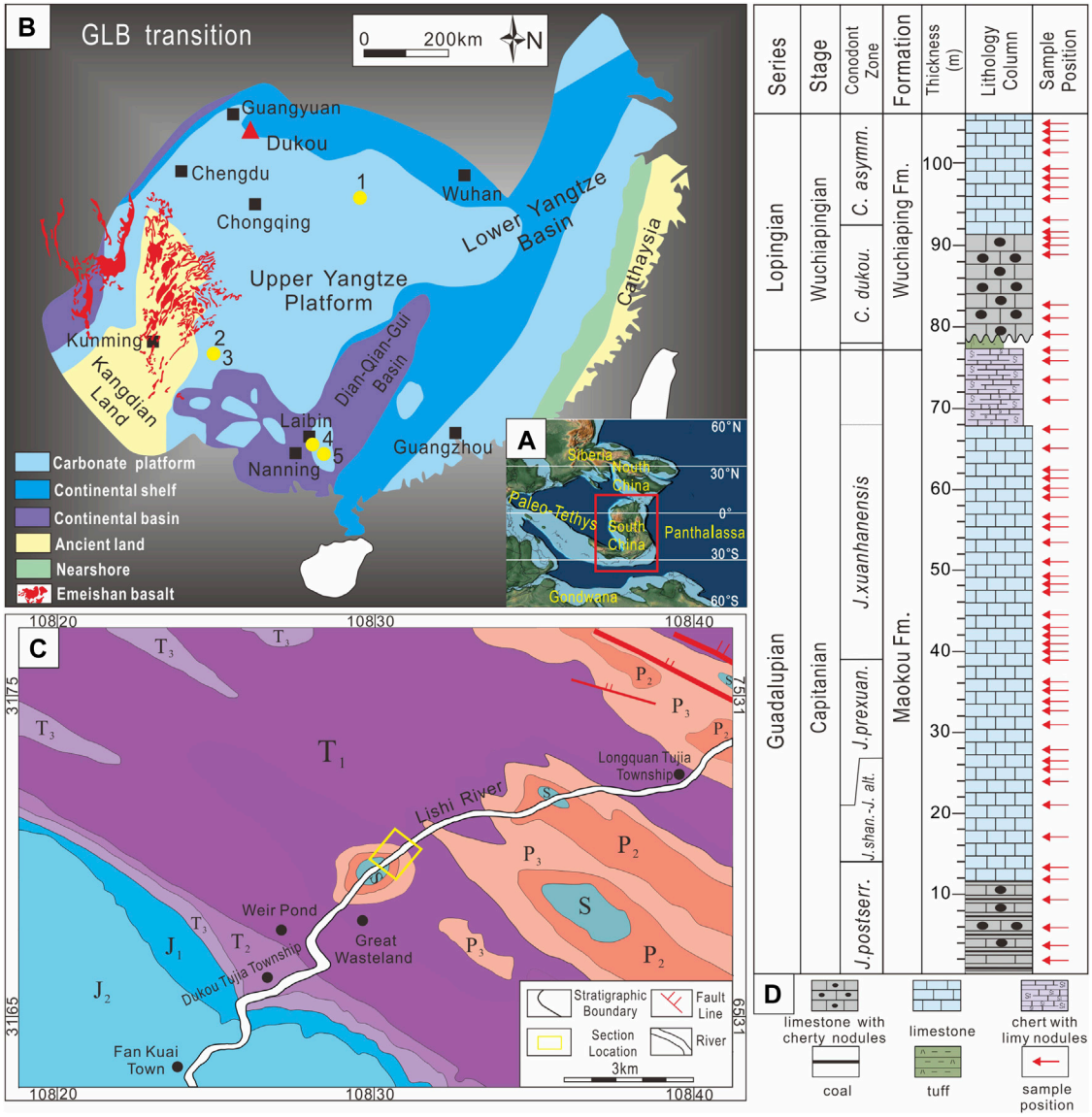

FIGURE 1
(A) Global paleogeographic map during the GLB transition (Scotese. 2016). **(B)** Paleogeographic map of South China in the GLB transition, modified from Yao et al. (2015) (1. The Rencunping section 2. The Xiong Jiachang section 3. The Gouchang section 4. The Tieqiao section 5. The Penglaitan section) **(C)** Geological map of the study area (J_3 = Upper Jurassic, J_2 = Middle Jurassic, J_1 = Lower Jurassic, T_3 = Upper Triassic, T_2 = Middle Triassic, T_1 = Lower Triassic, P_3 = Upper Permian, P_2 = Middle Permian, S = Silurian). **(D)** Lithologic stratigraphy of the upper Maokou Formation and the lower Wuchiaping Formation at the Dukou section. The conodont biostratigraphy of the investigated section is based on Mei et al. (1994a, 1994b), Yuan (2015) and Shen et al. (2020). Abbreviation: *J. postserr.=Jinogondolella postserrata* zone, *J. shan.=Jinogondolella shannoni* zone, *J. alt.= Jinogondolella altudaensis* zone, *J. prexuan.=Jinogondolella prexuanhanensis* zone, *J. xuanhanensis.=Jinogondolella prexuanhanensis* zone, *C. dukou.=Clarkina dukouensis* zone, *C. asymm.= Clarkina asymmetrica* zone.

The upper Maokou Formation (Capitanian sequence, 0–77 m) and lower Wuchiaping Formation (Early Wuchiapingian sequence, 77–106 m) consist of this study carbonate succession at the Dukou section. The lithology of the studied succession is dominated by light-gray micrite limestone, and the lower part of the Capitanian and Wuchiaping sequences are dark-grey limestone with cherty nodules (Figure 1D). It should be pointed out that that 9 m thick black chert with limy nodules appeared at the top of the Capitanian sequence, and this silica unit is also called the "Kuhfeng Chert Unit" (Qiu and Gu, 1991; Mei et al., 1994a; Hu, 2000). The lithological GLB can be placed at the base of the yellow-green clay rock (Wangpo Shale), the Wangpo Shale is also recognized across South China as the lithological boundary of GLB (Shen et al., 2013; Cao et al., 2018).

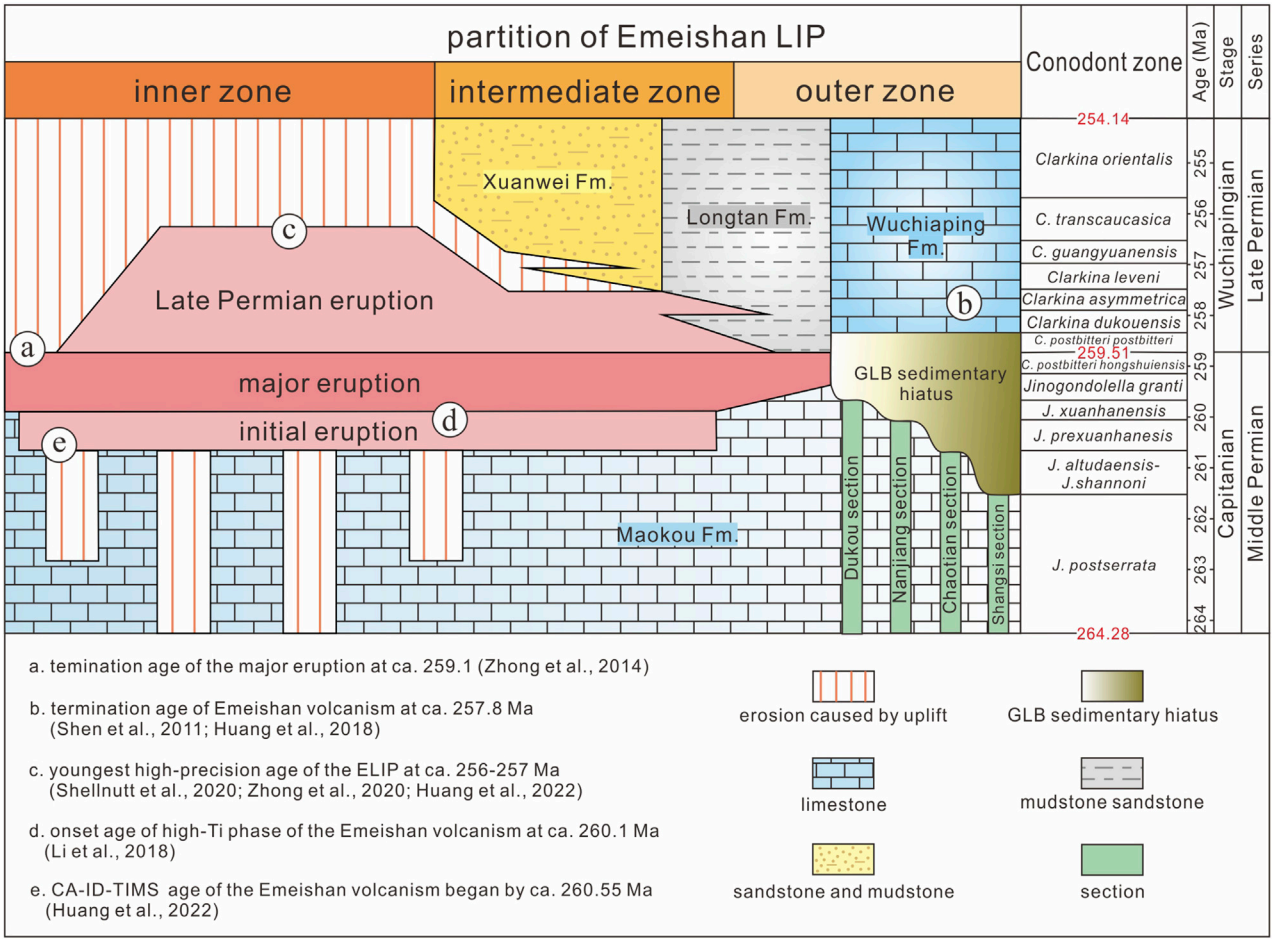

FIGURE 2
GLB lithostratigraphic sedimentary sequence (Wang et al., 2020), spatial-temporal distribution of the Emeishan LIP (Shen et al., 2011; Zhong et al., 2014, 2020; Li D. D. et al., 2018; Huang et al., 2018, 2022; Shellnutt et al., 2020), and GLB biostratigraphic correlation (Mei et al., 1994a; 1994b; Mei, 1995; Lai et al., 2008). Chronostratigraphic scale is according to Shen et al. (2022).

The global Late Guadalupian regression and eruption of Emeishan LIP in South China, and resulted in a widespread GLB sedimentary hiatus across most of South China (Mei, 1995; He et al., 2003; Haq and Schutter, 2008; Hou et al., 2020). In the southwestern part of South China, the Emeishan LIP, beginning in the late Guadalupian (Zhou et al., 2002; Shellnutt, 2014; Zhong et al., 2014), had a great influence on the Lopingian depositional system to the east. The terrestrial Xuanwei Formation developed landward of the intermediate zone, the transitional Longtan Formation developed the seaward of the intermediate zone, and the marine Wujiaping Formations mainly developed in the outer zone (Figure 2).

GLB marine strata succession in South China consists of the Maokou and Wuchiaping formations (Sun et al., 2010; Shen et al., 2019). Conodont biostratigraphy of South China indicates that the upper Maokou Formation and Wuchiaping Formation correspond to the Capitanian stage (264.28–259.51 Ma) and the Wuchiapingian stage (259.51–254.14 Ma), respectively (Shen et al., 2020, 2022). In the Upper Yangtze, compared with the Shangsi and Chaotian sections, the Dukou section retains four conodont zones in the Capitanian stage (Mei et al., 1994a; 1994b; Yuan, 2015; Shen et al., 2020) (Figure 1D, Figure 2), indicating that the sedimentary record is relatively complete.

Conodont biostratigraphic correlations from the marginal inner zone to the outer zone of the Emeishan LIP, shows that initial eruption began in the *J. altudaensis zone* of the middle Capitanian (261–262 Ma), and dramatically increased in extent and volume in the *J. xuanhanensis zone* (260–261 Ma) (Sun et al., 2010; Shen et al., 2019). Increasingly reported high-precision U-Pb ages (Shen et al., 2011; Zhong et al., 2014, 2020; Li Y. et al., 2018; Huang et al., 2018; Shellnutt et al., 2020; Figure 2) constrained the Emeishan LIP to Late Capitanian-Early Wuchiapingian (approximately 261–257 Ma). The new CA-ID-TIMS U-Pb ages from the Binchuan area of inner zone demonstrate that Emeishan volcanism began by 260.55 ± 0.07 Ma and persisted until at least 257.22 ± 0.37 Ma (Huang et al., 2022; Figure 2).

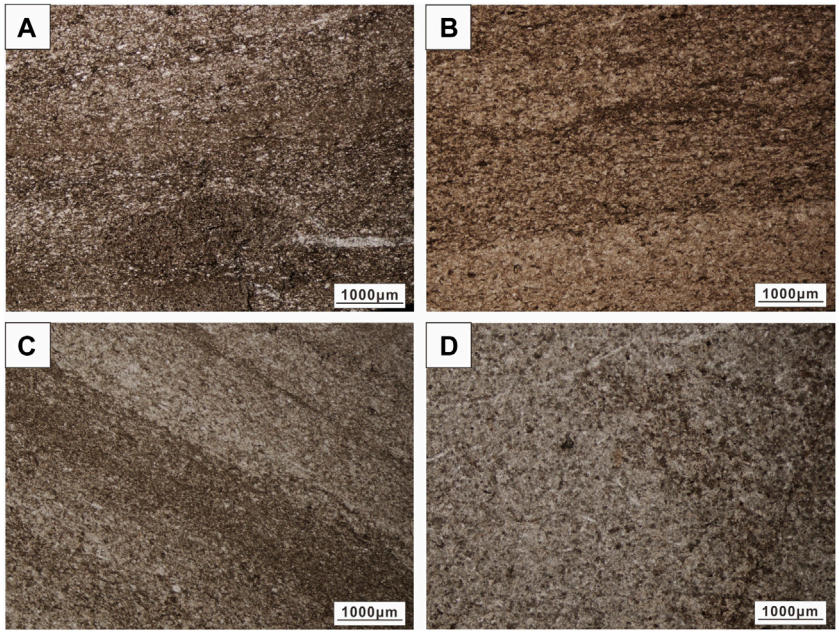

FIGURE 3
Photomicrographs of micritic to near-micritic carbonates. **(A–D)**: Samples DK-14, DK-32, DK-51, and DK-60).

3 Samples and methods

3.1 Sample preparations

Under the petrographic observation of thin sections, avoided carbonate grains (e.g., peloids and bioclasts), only micrite component was sampled (Figure 3). A total of 56 carbonate samples were collected from the Dukou section, of which 40 samples were from the Capitanian succession and 16 samples were from the Wuchiapingian succession. The specific sampling locations can be seen in Figure 1D.

To further minimize the influence of diagenesis on the geochemical signatures, samples were crushed into mm-sized particles to eliminate contamination from the cement veins and recrystallized spots. Samples were ground to 200 mesh in an agate mortar and three subsets were prepared for 1) $\delta^{13}C_{carb}$ and $\delta^{18}O$, 2) $^{87}Sr/^{86}Sr$ ratios, and 3) trace element analyses.

3.2 Methods

3.2.1 Carbon and oxygen isotopes

Carbon and oxygen isotopes (56 samples) were measured at the Nanjing Hongchuang Exploration Technology Service Co., Ltd, Nanjing, China. Isotope ratios are reported in per mil (‰) notation relative to the Vienna Pee Dee Belemnite standard (VPDB ‰). Samples were calibrated using China standards (GBW04405). The uncertainty (1σ) calculated from standards per run is typically 0.1‰.

3.2.2 $^{87}Sr/^{86}Sr$ ratios

A total of 56 samples were analyzed for $^{87}Sr/^{86}Sr$ ratios at the State Key Laboratory of Oil and Gas Reservoir Geology and Exploitation of the Chengdu University of Technology, China. The samples (50 mg each) were washed with deionized water, dried, and crushed to less than 0.0750 mm. The $^{87}Sr/^{86}Sr$ ratios were measured using a Thermo-Fisher Scientific Triton Plus mass spectrometer.

The measured $^{87}Sr/^{86}Sr$ ratios were normalized to an $^{86}Sr/^{88}Sr$ ratio of 0.1194 (Nier, 1938), calculated from 150 measurements. An internal precision of ~5×10^{-6} (relative SE) was maintained. The analytical precision was monitored using NBS 987 and the mean measured value obtained for NBS 987 was 0.710,247 ± 0.000008 [2σ, number of samples (n) = 6]. All reported $^{87}Sr/^{86}Sr$ data were corrected to the value of the international standard NBS 987 ($^{87}Sr/^{86}Sr$ = 0.710,248).

3.2.3 Trace elements

Major and trace elements (56 samples) were measured in Chengdu Oriental Mineral Development Technology Research Institute. Major elements were measured by ZSX Primus II X-ray fluorescence spectrometer. Trace element analysis was performed on an American PE 5300 V. The analysis process adopts China standards GBW07314, GBW07315,

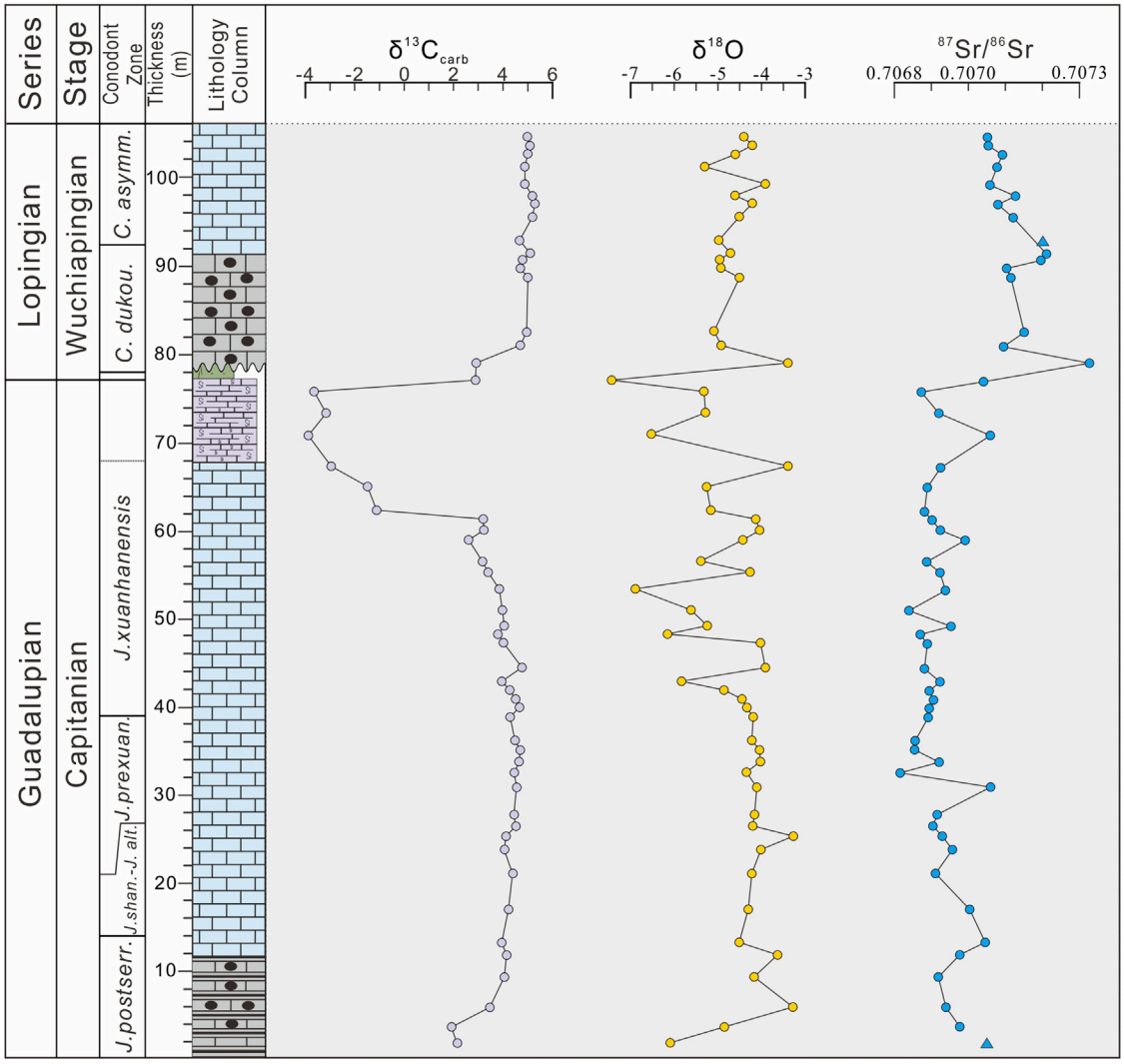

FIGURE 4
The profiles of carbon, oxygen and strontium isotopes of the Dukou section (The legend is shown in Figure 1D, the triangles are samples that may be affected by diagenesis) (The data of $\delta^{13}C_{carb}$ discussed here was published with no detail discussion in our previous paper, the lower 36 data points of Sr isotopes was published in our previous paper).

GBW07316 and USGS basalt standard material 6BHVO-2 for quality control, and uncertainty was generally better than 5%.

4 Results

4.1 Carbon and strontium isotopes

During the Capitanian, the $\delta^{13}C_{carb}$ presents large fluctuations (Figure 4), which varies from − 3.88‰ to + 5.3‰, with an average of + 3.5‰. In the Early Capitanian, the $\delta^{13}C_{carb}$ remains at a relatively stable high value of about + 4‰. In the Late Capitanian, the $\delta^{13}C_{carb}$ begins to decrease gradually after reaching a peak value of + 4.78‰, followed by a rapid negative drift which decreases from + 3.2‰ to − 3.9‰. This rapid negative drift is comparable to earlier studies (e.g., Shen et al., 2013, 2020; Yuan, 2015). In the Early Wuchiapingian, the $\delta^{13}C_{carb}$ quickly rises from − 3.9‰ to + 2.9‰, and remains at a high value of about + 5‰.

The $^{87}Sr/^{86}Sr$ ratios of the Dukou section also show significant fluctuations (Figure 4), which vary from 0.70682 to 0.70733, with an average of 0.70699. In the entire Capitanian, the $^{87}Sr/^{86}Sr$ ratios decrease rapidly from 0.70705 to 0.70682, and then remain around 0.70689. Subsequently, the $^{87}Sr/^{86}Sr$ ratios rise rapidly to around 0.70713 during the Early Wuchiapingian.

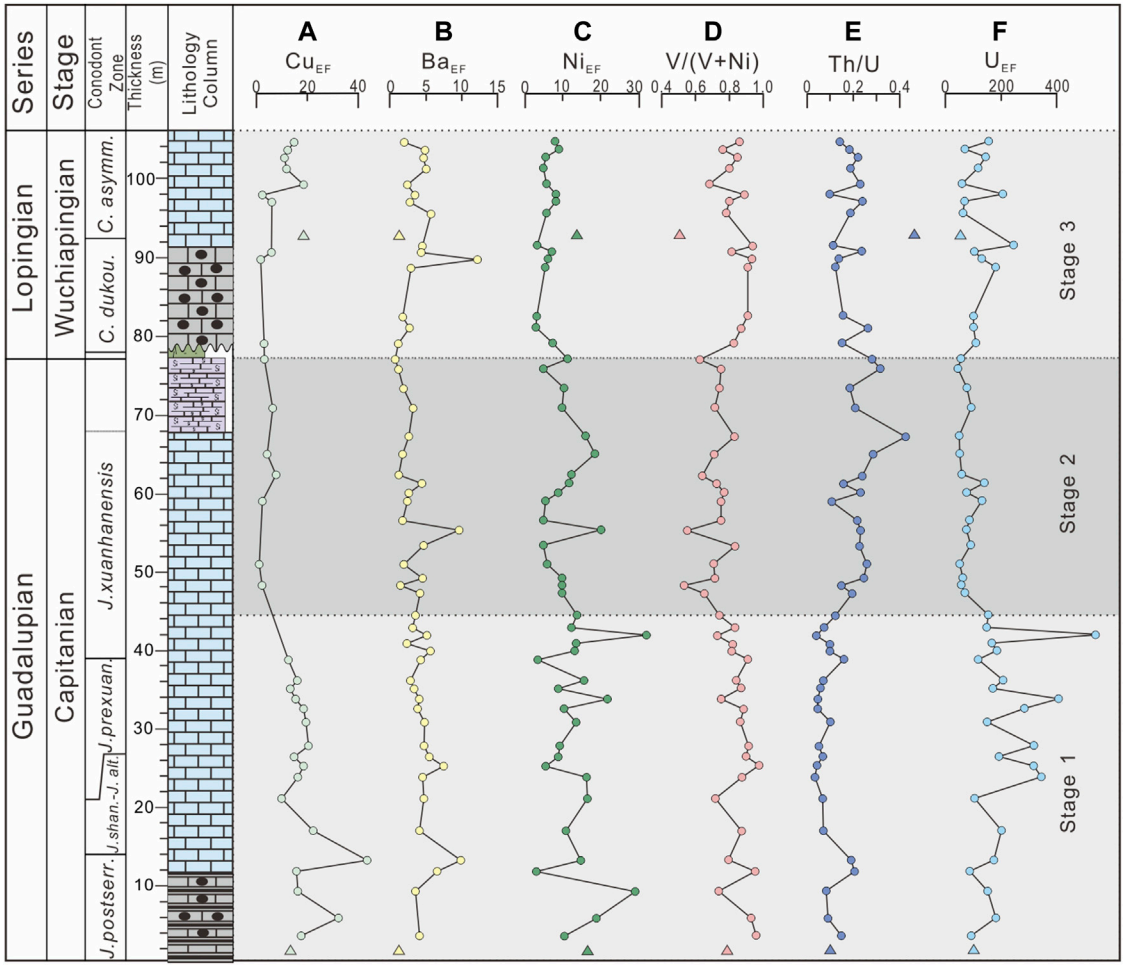

FIGURE 5
Profiles of **(A)** Cu_{EF}, **(B)** Ba_{EF}, **(C)** Ni_{EF}, **(D)** V/(V+Ni), **(E)** Th/U and **(F)** U_{EF} of Dukou section, the triangles are samples that may be affected by diagenesis.

4.2 Trace elements

The elemental geochemistry of the investigated carbonates includes the primary productivity (Cu_{EF}, Ni_{EF}, Ba_{EF}) and redox (V/(V+Ni), Th/U and U_{EF}) (Tribovillard et al., 2006; Shen et al., 2014; Takahashi and AuthorAnonymous, 2014). To normalize the results and describe the enrichment degree of the environmentally sensitive elements, enrichment factors (EF) of selected elements were calculated as: $X_{EF} = (X/Al)_{sample}/(X/Al)_{average\ shale}$, where X and Al represent the concentrations of the element of interest and the concentrations of average shale are from Wedepohl (1971, 1991). Their profiles are shown in Figure 5 and results are listed in Supplementary Table S1.

According to the systematic variations of trace elements of the Dukou section (Figure 5), we divide it into three stages. The Cu_{EF} gradually decreases after reaching the maximum in Stage 1, and remains stably low in Stage 2 and the beginning of Stage 3, and subsequently increases. Except that some samples increase in Stage 2, the variation of Ba_{EF} is similar to that of Cu_{EF}. Ni_{EF} fluctuates dramatically in Stage 1 and reaches the maximum at the end of this stage. At the beginning of Stage 2, Ni_{EF} declines slowly, follows by two subsequent rises, and increases slightly at the end of this Stage. It decreases slowly at the beginning of Stage 3, and gradually increases after stabilization. The value of Ni_{EF} in Stage 1 is higher than in Stages 2 and 3. In general, the primary productivity proxies seem to exhibit a downward trend in Stage 2. Both V/(V+Ni) and U_{EF} decrease in Stage 2 and remain at a certain range, which is consistent with the increase of Th/U in Stage 2.

5 Discussions

5.1 Evaluation of sample preservation

Diagenetic alteration of marine carbonates has been documented to significantly alter the primary geochemical

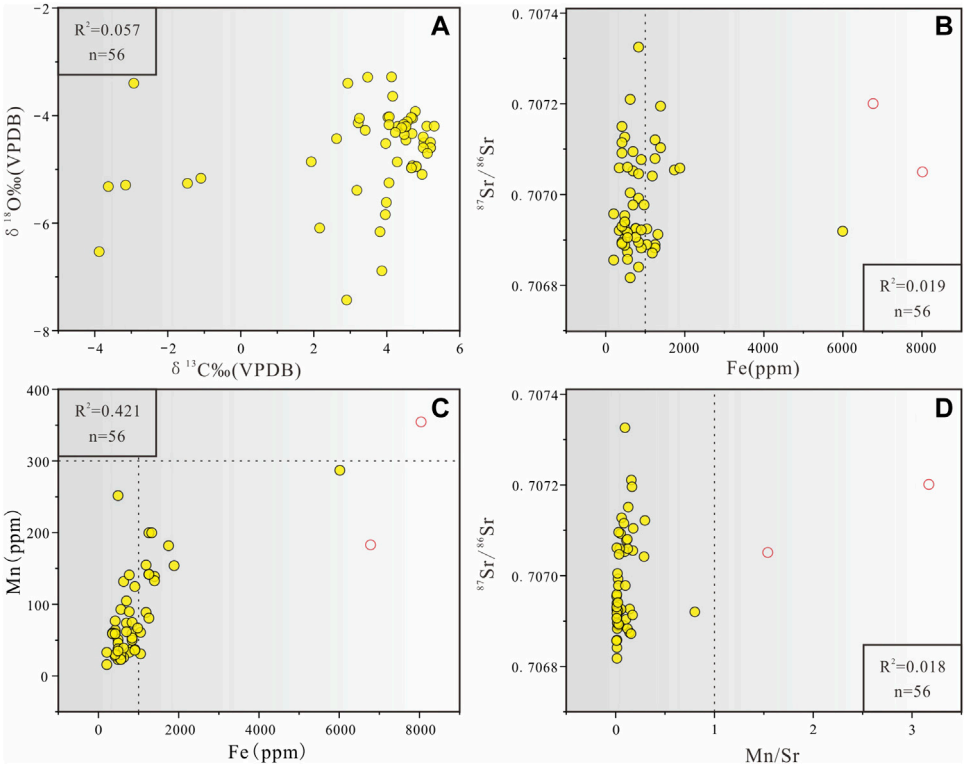

FIGURE 6
Scatter diagrams showing correlations of **(A)** $\delta^{13}C_{carb}$with $\delta^{18}O$, **(B)** Fe with $^{87}Sr/^{86}Sr$, **(C)** Fe with Mn, and **(D)** Mn/Sr with $^{87}Sr/^{86}Sr$ in the investigated Dukou section (Red rings indicate data may have been affected by diagenesis).

signatures (Veizer, 1983), and the evaluation of carbonate preservation is therefore the foundation needed for the reconstruction of reliable chemostratigraphic profiles and interpretation of the paleoenvironmental conditions. Previous paleoenvironmental studies suggested that the diagenetic alteration at low water/rock interaction ratios, as reflected by minimum recrystallization, does not dramatically alter the signatures of the paleoenvironmental proxies (Veizer, 1983; Azmy et al., 2011). Because the diagenetic fluids are composed of water, the $\delta^{18}O$ is also significantly decreased during diagenesis but the $\delta^{13}C$ is relatively less susceptible to alteration since the diagenetic fluids do not usually have highly dissolved CO_2 to reset the C-isotope signatures of carbonates unless organic matter is involved (Cochran et al., 2010; Saltzman and Thomas, 2012).

Therefore, the $\delta^{18}O$ values are utilized as a reliable proxy for evaluating the degree of geochemical preservation of carbonates. It is generally believed (Derry et al., 1992; Kaufman and Knoll, 1995) that samples with $\delta^{18}O$ values greater than—eight‰ are commonly accepted as pristine ones. Additionally, the post diagenesis of marine carbonate rocks could cause the simultaneous change of $\delta^{13}C_{carb}$ and $\delta^{18}O$, which led to a positive correlation between $\delta^{13}C_{carb}$ and $\delta^{18}O$ (Veizer et al., 1999; Knauth and Kennedy, 2009). However, our data show $\delta^{18}O$ values greater than—eight‰ and a poor correlation coefficient between $\delta^{13}C_{carb}$ and $\delta^{18}O$ (R^2 = 0.057; Figure 6A). Thus, obvious diagenesis is not supported by the data.

The poor correlation coefficient between Fe contents and $^{87}Sr/^{86}Sr$ values (R^2 = 0.019; Figure 6B) and the poor correlation coefficient between Fe contents and Mn contents (R^2 = 0.421; Figure 6C) suggest a high degree of preservation of near-primary signatures. Additionally, the investigated carbonates have generally low Mn contents (16–355 ppm; Supplementary Table S1) and high Sr contents (58–3880 ppm; Supplementary Table S1), and the Mn/Sr ratios (mainly < 1) exhibit a poor correlation coefficient with their $^{87}Sr/^{86}Sr$ values (R^2 = 0.018; Figure 6D), also implying insignificant contributions from diagenetic fluids (Li et al., 2021).

As mentioned above, diagenetic alteration of carbonates with progressive burial results in a dramatic depletion in the Sr contents but enrichment in other elements. (Veizer, 1983; Derry et al., 1992; Denison et al., 1994; Li, 2016). Therefore, the Sr ratios are utilized as a dependable proxy for evaluating the degree of geochemical preservation of carbonates. The poor correlations (R^2= 0.099 to 0.001) of Sr with the other proxies (e.g., V/(V+Ni), Th/U, Cu, Ba, Ni, U; Figure 7A–F;

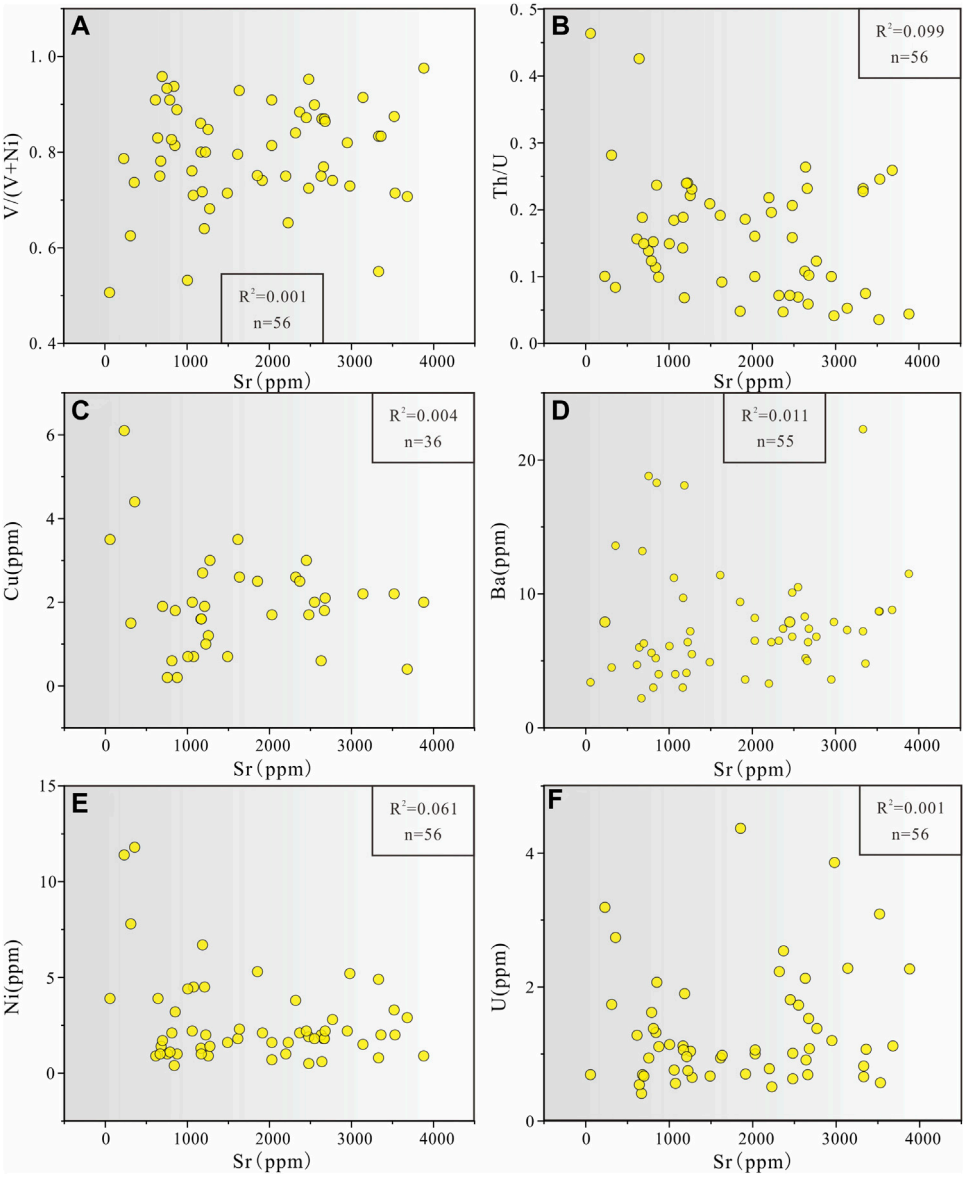

FIGURE 7
Scatter diagrams showing correlations of Sr with **(A)** V/(V+Ni), **(B)** Th/U, **(C)** Cu, **(D)** Ba, **(E)** Ni, and **(F)** U in the investigated Dukou section.

Supplementary Table S1) suggest that the studied carbonates succession retain at least near-primary geochemical signatures. (e.g., Shembilu and Azmy, 2022).

5.2 The negative drifting of $\delta^{13}C_{carb}$ during the GLB transition

The $\delta^{13}C_{carb}$ values in the Early Capitanian retain relatively high (~ +4.5‰) positive plateau. The Cu_{EF}, Ba_{EF}, and Ni_{EF} reveal that there is indeed a relatively high marine primary productivity during the Early Capitanian. Then, the value of $\delta^{13}C_{carb}$ shift to a slight negative drifting at around 261.6 Ma. Meanwhile, the primary productivity proxies occurred a slight downward decline. The redox indicators (V/(V+Ni), Th/U and U_{EF}) recorded in this carbonate platform reflect increased oxidation of surface seawater, which is opposite to the deep water facies that was anoxia and intermittent euxinia evidenced by the coincidence between reduction of framboid size and the extremely negative sulfur isotope values of pyrite (Wei et al., 2016, 2019). To around 260.4 Ma in the Late Captanian, a rapid $\delta^{13}C_{carb}$ negative shift occurred, and also had a synchronous

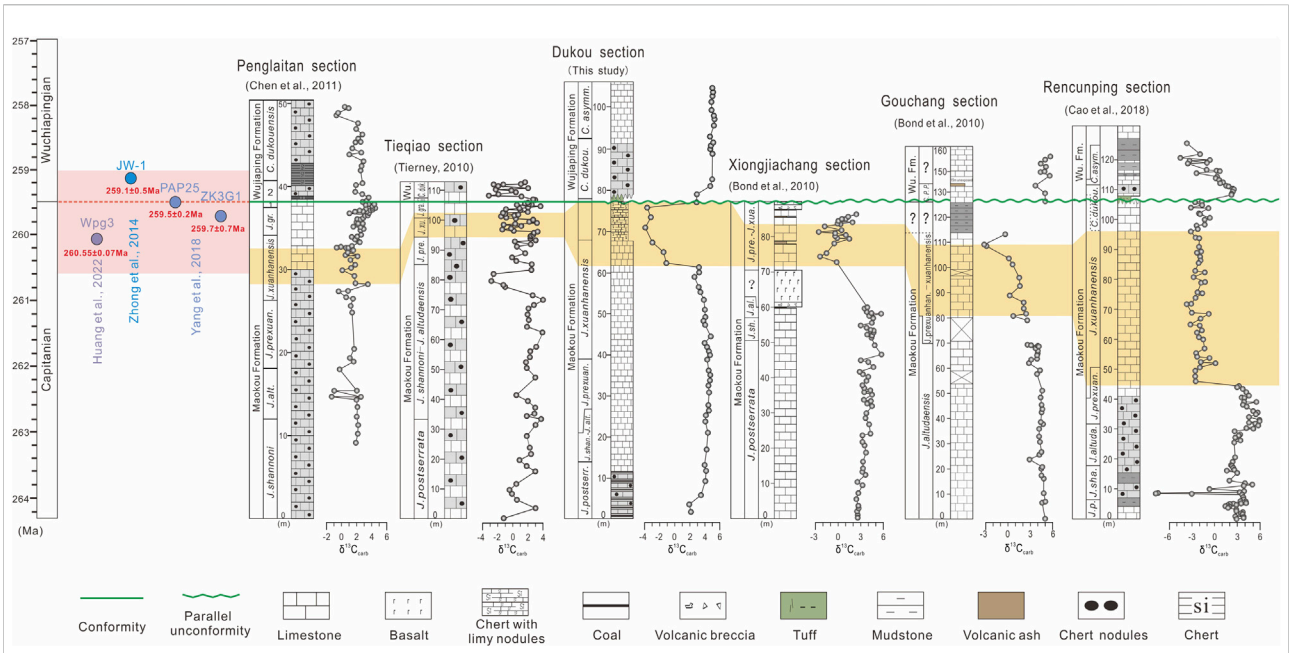

FIGURE 8
Carbon isotope chemostratigraphy of the South China during the GLB transition. The reported high-precision zircon U-Pb age data of the Emeishan LIP are from Zhong et al. (2014); Yang et al. (2018); Huang et al. (2022). The reported carbon isotope data: Penglaitan section is from Chen et al. (2011); Tieqiao section is from Tierney. (2010); Xiongjiachang and Gouchang sections are from Bond et al. (2010); Rencunping section is from Cao et al. (2018). The age of Capitanian is from JTS-2022. 1 = *Clarkina postbitteri hongshuiensis*, 2 = *Clarkina postbitteri postbitteri*.

response in other regions (Figure 8). Rencunping section in Hunan exhibits two significant negative $\delta^{13}C_{carb}$ drifts during the Capitanian (Cao et al., 2018), a negative $\delta^{13}C_{carb}$ drift in the *J. shannoni* zone is related to dolomitization to degree, and that of it in the J. xuanhanensis zone (from + 5‰ to − 2‰) is still primary signal; Xiongjiachang section in Guizhou displays a rapid negative $\delta^{13}C_{carb}$ drift (from + 4‰ to − 3‰) in the *J. prexuanensis-J.xuanhanensis* zone, and neary Gouchang and Houchang sections also show similar negative drift (Bond et al., 2010); Penglaitan and Tieqiao sections of Guangxi presents two significant negative $\delta^{13}C_{carb}$ drifts in the *J. altudaensi* zone and the *J. xuanhanensis* zone respectively (Tierney, 2010), the latter may correspond to the $\delta^{13}C_{carb}$ negative drift in the late Capitanian.

Through investigating volcano-sedimentary record of southwest China, Wignall et al. (2009) revealed that the rapid $\delta^{13}C_{carb}$ negative drift coincided with the onset of Emeishan volcanism. According to the ages of conodont biostratigraphy, Sun et al. (2010) proposed that eruption of Eemishan LIP started from the *J. altudaensis* zone and peaked in the *J. xuanhanensis* zone. Recently, the new CATIMS U-Pb ages result accurately confirm that the onset time of Eemishan LIP was 260.55 ± 0.07 Ma (Huang et, al., 2022), and the peak time was ~ 260 Ma (Zhong et al., 2014; Yang et al., 2018). The onset time of the $\delta^{13}C_{carb}$ negative drift in this study is consistent with that of the Emeishan volcanic eruption (Figure 8), indicating that Emeishan LIP is undoubtedly one of the important mechanisms driving the $\delta^{13}C_{carb}$ negative drift. Meanwhile, the Cu_{EF}, Ba_{EF}, and Ni_{EF} in this interval recorded a decline of marine primary productivity, and V/(V+Ni), Th/U, and U_{EF} reveal an enhanced oxidation of seawater, which could promote this $\delta^{13}C_{carb}$ negative drifting together.

In contrast to the magma eruption scale in Siberia LIP (4×10^6 km^3) and Deccan LIP ($2–3 \times 10^6$ km^3), a total amount of magma in Emeishan LIP is relatively small ($0.3–0.6 \times 10^6$ km^3; Shellnutt., 2014), which is might not enough to cause such a large $\delta^{13}C_{carb}$ negative drift. In addition to volcanic outgassing, thermal decarbonation reactions also produces a large amount of greenhouse gases. It has been suggested that Emeishan volcanism caused the upwelling of magma to bake the underlying the host sediments (mostly carbonates) to form a large amount of ^{13}C-poor CO_2 and CH_4, which entered the atmosphere in a short period (Svensen et al., 2007, 2009; Aarnes et al., 2010; Shellnutt et al., 2012). The widespread volcanic arcs and the initial breakup of Pangea may play an important role in the $\delta^{13}C_{carb}$ negative drift during the GLB transition (Maruyama et al., 2007; Macdonald et al., 2019; Zhang et al., 2022b). In addition, in the context of global regression (Ross and Ross, 1987; Haq and Schutter, 2008), the redox indictors (V/(V+Ni), Th/U and U_{EF}) of this study indicate enhanced marine oxidation in the Late Capitanian. Therefore, the decline of sea-level may cause exposure of continental shelves

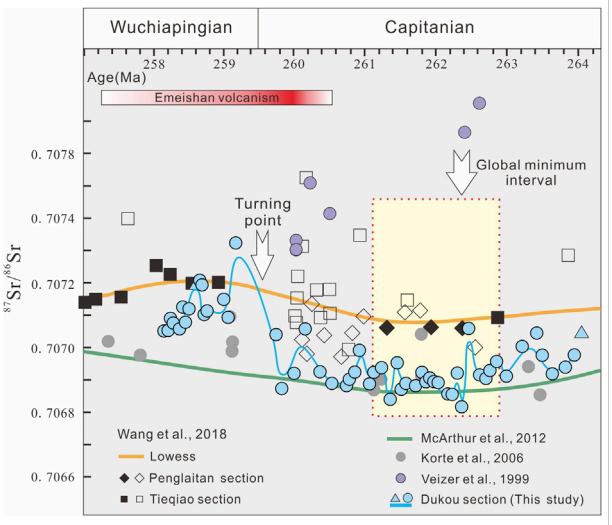

FIGURE 9
The profile of $^{87}Sr/^{86}Sr$ during the GLB transition. Note: The data of the Dukou section are from this study and other data are from Veizer et al. (1999), Korte et al. (2006), McArthur et al. (2012) and Wang et al. (2018).

and re-oxidization of ^{12}C-rich organic matter, which will promote such large magnitude of negative drift to some extent.

The $\delta^{13}C_{carb}$ values increased rapidly around 259.4 Ma, which can be observed in the Rencunping, Shangsi, Chaotian and Tieqiao sections of South China (Tierney, 2010; Jost et al., 2014; Cao et al., 2018), as well as the sections in Armenia, Turkey, and Europe (Baud et al., 1989; Jost et al., 2014). The cause of this $\delta^{13}C_{carb}$ positive drift is considered to be linked to the consumption of atmospheric pCO_2 of low latitude mafic weathering (Emeishan basalt), which led to the onset of the Permian P4 glacial (Yang et al., 2018; Sun et al., 2022).

5.3 Dominant cause of $^{87}Sr/^{86}Sr$ ratios' variation during the GLB transition

The strontium isotope variations of this study are consistent with that reported previously (Figure 9; Veizer et al., 1999; Korte et al., 2006; McArthur et al., 2012; Wang et al., 2018). The $^{87}Sr/^{86}Sr$ ratios of the Dukou section remained low during the Middle-Late Capitanian, reaching the globally recognized minimum value (0.70682) at approximately 262 Ma (Figure 9). Until approximately 259.4 Ma, the $^{87}Sr/^{86}Sr$ ratio also showed a significant recovery (Figure 9).

Prior to the rapid increase of $^{87}Sr/^{86}Sr$ ratios, the long-term slow-declining low value indicated the dominant role of mantle-derived Sr Emeishan basalt eruption was considered to be the possible cause of the decrease in the seawater $^{87}Sr/^{86}Sr$ ratios (Huang H. et al., 2019; Li et al., 2021). However, the minimum of $^{87}Sr/^{86}Sr$ ratio is inconsistent with the duration of the Emeishan LIP (Zhong et al., 2014, 2020; Huang et al., 2018, 2022). It is intriguing that larger Siberian LIP during the end-Permian did not cause such a significant decrease of $^{87}Sr/^{86}Sr$ ratios (McArthur et al., 2012, 2020; Liu et al., 2013). Therefore, it should be due to other causes that the mantle-derived Sr flux has long been dominant.

From a longer-time scale, the decline of $^{87}Sr/^{86}Sr$ ratio during the LPIA has already begun since the Late Carboniferous (McArthur and Howarth, 2004; Kani et al., 2013; Wang et al., 2018). Glacial maximum period (Late Carboniferous-Early Permian) could explain the decrease of crustal-derived Sr to some extent (Chen et al., 2018; Chen et al., 2022). However, it is difficult to provide a reasonable explanation for the continuous decline of $^{87}Sr/^{86}Sr$ ratios within the glacial continuous weakening process (Middle Permian).

The dominance of mantle-derived Sr flux could be the important reason for the long-term decline of $^{87}Sr/^{86}Sr$ ratios and the minimum value during the Capitanian. This period coincided with the transition from convergence to the disintegration of the Pangea. The Arc volcanism with plate movement (Macdonald et al., 2019), active oceanic ridge magmatism (Zhang B. L. et al., 2021), and their related mafic weathering should provide considerable mantle-derived Sr flux. Marine hydrothermal cherts during the Capitanian were widely distributed in the northern margin of the Upper Yangtze (Murchey and Jones, 1992; Qiu and Wang 2011; Dong et al., 2020), supporting the enhanced supply of mantle-derived material. The long-term low $^{87}Sr/^{86}Sr$ value of Dukou section increase rapidly from approximately 259.4 Ma (Figure 9), which corresponds to the attenuation period of weathering intensity. It is difficult to explain this recovery with the change of the crust-derived Sr flux. A significant reduction in mantle-derived Sr flux might mainly be attributed to the rapid weakening of oceanic ridge and arc volcanism associated with active global-scale crust-mantle interaction. In summary, the strontium isotopic composition of this period is more dominated by mantle-derived Sr flux.

5.4 The integrated geochemical indices indicating the co-evolution of climate-ocean-biodiversity system during the GLB transition

The linkage between LIP volcanism and biological crisis events has long been a very interesting topic (Courtillot, 1999; Wignall, 2001; Courtillot and Renne, 2003; Chen and Xu, 2019). Large-scale volcanic activity will release a large amount of volcanic ash, toxic gases, and greenhouse gases in a short period, ultimately leading to environmental degradation and biological crisis (Bond et al., 2010; Day et al. al., 2015; Fan et al., 2020). Based on cases such as the temporal coincidence

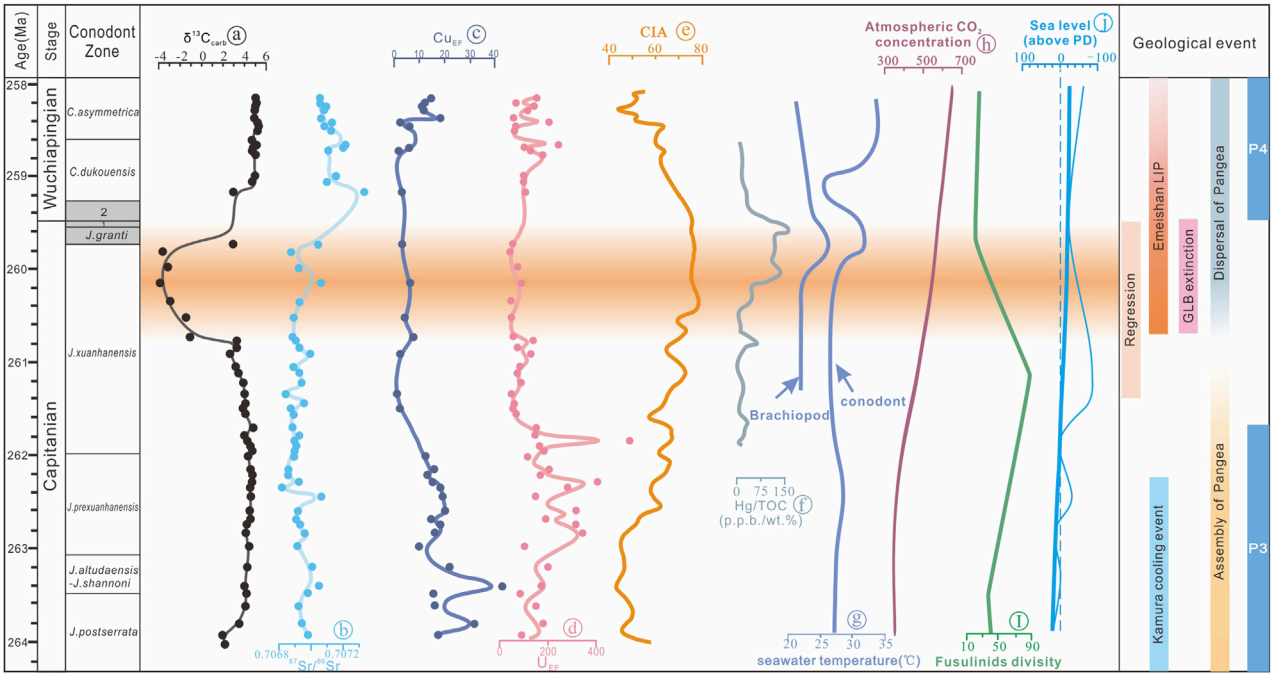

FIGURE 10
Paleoenvironmental indicators and geological events during the GLB transition. The profiles of $\delta^{13}C_{carb}$, $^{87}Sr/^{86}Sr$, Cu_{EF}, and U_{EF} are from the study of the Dukou section, and the CIA values are from Sun et al. (2022), Hg/TOC ratios are from Huang Y. G. et al. (2019), relative seawater temperature is based on $\delta^{18}O$ composition in conodonts and brachiopods from Chen et al. (2011) and Wang et al. (2020). The atmospheric CO_2 concentration is from Foster et al. (2017), warm-water benthic foraminifer diversity from Davydov, (2014), global sea-level change from Haq and Schutter (2008). Geological event: Emeishan LIP (Shellnutt et al., 2012; Zhong et al., 2014; Huang et al., 2018), the GLB extinction (Wignall et al., 2009; Huang Y. G. et al., 2019; Shen et al., 2020), the Kamura events (Isozaki et al., 2007, 2011), dispersal and assembly of Pangea (Maruyama et al., 2007; Isozaki, 2009; Santosh et al., 2009; Shen et al., 2019). The duration of P3-P4 glacial (Metcalfe et al., 2015), sea-level change (Haq and Schutter, 2008). Abbreviations: P3 = the third stage of Permian glaciation, P4 = the fourth stage of Permian glaciation, 1 = *Clarkinapostbitteri hongshuiensis*, 2 = *Clarkina postbitteri postbitteri*, geological age and conodont biostratigraphy is based on Shen et al. (2019) and Shen et al. (2022).

between the end-Permian mass extinction and the eruption of the Siberian LIP, large-scale volcanic activity is considered to be one of the important factors of the extinction (Burgess and Bowring, 2015; Chen and Xu, 2019).

The GLB transition also experienced a significant extinction event (Jin et al., 1994; Shen and Shi, 1996, 2002; Wignall et al., 2009), which was called " end-Guadalupian mass extinction". The extent of this extinction event has been controversial (Jin et al., 1994; Stanley and Yang, 1994; Shen and Shi, 1996, 2002; Wignall et al., 2009; Huang Y. G. et al., 2019). However, the decline in the diversity of shallow-marine invertebrates (including corals, brachiopods and ammonoids) still reflects that this extinction event is indisputable (Wang and Sugiyama, 2000; Groves and Wang, 2013; Shen et al., 2020). The trace elements of the samples from the Dukou section show that the enrichment factors such as Cu_{EF}, Ba_{EF}, and Ni_{EF} decreased accompanied by a $\delta^{13}C_{carb}$ negative drift in the Late Capitanian (Figure 7), indicating a decrease in marine primary productivity. This decline is in good chronological agreement with the previously proposed GLB biocrisis.

Wignall et al. (2009) proposed that the Emeishan volcanic activity might trigger a biological extinction event based on the temporal coincidence among Emeishan volcanism, biocrisis and carbon isotope negative drift. Bond et al. (2010) reported the loss of keriothecal-walled fusulinaceans and a turnover in calcareous algae in the Upper Maokou Formation at the Xiongjiachang section, and carbonate deposition was frequently interrupted by thick volcanic ash depositional events, revealing a potential link between Emeishan volcanism and biological extinction. The sedimentary, paleoecologic, and geochemical analysis of the Penglaitan section show collapse of metazoan reef system, with two abnormally high mercury concentration/total organic carbon (Hg/TOC) ratios during the GLB transition, supporting that the Emeishan LIP may trigger biotic extinction (Figures 10–f; Huang Y. G. et al., 2019). Accumulating evidence shows that the Emeishan LIP may be one of the important mechanisms of the end-Guadalupian biocrisis (Wignall et al., 2009; Bond et al., 2010; Chen et al., 2011; Chen and Xu, 2019; Sun et al., 2022). Here, we collected a series of paleoenvironmental indicators to integrate our results and carried out a global-scale comprehensive comparative analysis (Figure 10).

A significant $\delta^{13}C_{carb}$ negative shift during the GLB transition is consistent with the onset of the Emeishan eruption and the initial breakup of the Pangea. This temporal consistency implies that it is related to the carbon-cycle disturbance caused by the global volcanic-tectonic activity, and is consistent with the GLB extinction. The $^{87}Sr/^{86}Sr$ ratios discussed above is dominated by the mantle-derived Sr flux, which also indicates that the global volcanic-tectonic activity caused by Earth's internal dynamics is the triggering factor for this biocrisis event. Declines in biodiversity are often a precursor to extinction events (Stanley, 2016). Biodiversity decreased significantly during the Emeishan LIP (Chen et al., 2011; Davydov, 2014; Zhang B. L. et al., 2021). In particular, the latest high-resolution paleontological data strongly confirms that species diversity declined rapidly during the Late Capitanian (Fan et al., 2020).

The reconstructed atmospheric CO_2 curve reveals there was a transient climate warming event in Late Capitanian (Figures 10–h; Foster et al., 2017). Meanwhile, the conodont $\delta^{18}O_{apatite}$ results of the Penglaitan section show that the seawater temperature increased about 6 ~ 8 °C (Figures 10–g; Chen et al., 2011), and the brachiopod $\delta^{18}O_{calcite}$ results of the Xikou section show that the seawater temperature increased about 4°C (Figures 10–g; Wang et al., 2020), both revealing a significantly transient warming event. Recently, the CIA curve established by the acid-insoluble residues of carbonate rocks (Figures 10–e; Sun et al., 2022), compared with the latest high-precision age of the Emeishan LIP (Huang et al., 2022), supporting a high-temperature plain in the main peak period (approximately 260 Ma), which may represent a transient warming event (Figure 10). This climate event may have been an important cause of the end-Guadalupian crisis. The redox proxies from this study support there was an enhanced seawater oxidation during the Late Capitanian (Figures 10–d), the onset of that is consistent with the end of the P3 glacial. Thereafter it in turn transitions to a reductive increase from the onset of P4 glacial. Obviously, the transient climate warming may be an important reason for the enhanced oxidation of the shallow-water shelf during this event, and inhibit the preservation of organic matter, which is precisely coupled with the carbon isotope negative drift. In contrast to the enhanced oxidation of the shallow-water shelf represented by the Dukou section, due to the transient climate warming, the ocean circulation may have weakened associated with a decrease in the temperature difference between high and low latitudes. Deep-water facies beyond the shelf may exacerbate oceanic water column stratification and marine anoxia, and even euxinia are not conducive to the survival and reproduction of organisms (Yan et al., 2013; Wang et al., 2022).

It was discussed previously that the onset of $\delta^{13}C_{carb}$ negative drifts and the strontium minimum was inconsistent during the Capitanian (Figure 10). However, across the GLB boundary, both showed a rapid positive drift almost simultaneously, and paced climate transition from interglacial to P4 glacial (Frank et al., 2015; Metcalfe et al., 2015; Davydov et al., 2022). But the eruption of the Emeishan LIP was not completely over, and the climate transitioned into the P4 glacial quickly. This may be due to the weathering of low-latitude mafic rocks and the possible volcanic ash aerosol effect (Huang et al., 2018; Yang et al., 2018), which led to the climate cooling. Consequently, the enrichment factors for trace elements in our study showed that primary productivity went into a tendency of recover in the Early Wuchiapingian, which proves that the biocrisis had been temporarily alleviated (Figures 10–c). (Azmy and Lavoie, 2009, Azomani et al., 2013, Kaufman et al., 1992, Shen and Mei, 2010)

6 Conclusion

1) The $\delta^{13}C_{carb}$ curve of the Dukou section has a significant shift during the GLB transition, and a negative drift in the Late Capitanian recorded the carbon-cycle perturbation event promoted by primary productivity proxies and redox condition initially. The surge of Emeishan LIP, contemporaneous volcanic arcs and local re-oxidized organic matter under the regression setting may be an superimposed factor for the later rapid negative drift.
2) The $^{87}Sr/^{86}Sr$ ratios of the Dukou section remained long-term low values during the entire Capitanian, reached a global minimum value around 262 Ma and appeared a significant increase till approximately 259.4 Ma. Fluctuations of strontium isotopic composition are more dominated by mantle-derived Sr flux.
3) The composited geological records of the climate-ocean system during the GLB transition, promoted carbon cycling perturbation and triggered the end-Guadalupian biocrisis.

Data availability statement

The original contributions presented in the study are included in the article/Supplementary Material, further inquiries can be directed to the corresponding authors.

Author contributions

RL, Writing–original draft, investigation, data curation. SS, Conceptualization, writing–review and editing, Investigation. WX, Data curation, investigation. AC, Conceptualization, writing–review and editing, Supervision, funding acquisition. JO, Reviewing. SY, Investigation. SX, Supervision. ZL, Reviewing. DY, Data curation. MH, Conceptualization.

Funding

This study was supported by the National Natural Science Foundation of China (Grant No. 42272132, No. 42172119 and No. 42050104), the Everest Scientific Research Program of

Chengdu University of Technology (Grant No. 2022ZF11402).

Acknowledgments

We thank reviewers and editors for their constructive reviews, and thank Wen Li, Haotian Luo, Ouwen Yang, Fuxiang Li, Yifan Huang for their helpful field works.

Conflict of interest

The authors declare that the research was conducted in the absence of any commercial or financial relationships that could be construed as a potential conflict of interest.

Publisher's note

Supplementary material

The Supplementary Material for this article can be found online at: https://www.frontiersin.org/articles/10.3389/feart.2022.1077017/full#supplementary-material

References

Aarnes, I., Svensen, H., Connolly, J. A. D., and Podlachikov, Y. Y. (2010). How contact metamorphism can trigger global climate changes: Modeling gas generation around igneous sills in sedimentary basins. *Geochimica Cosmochimica Acta* 74, 7179–7195. doi:10.1016/j.gca.2010.09.011

Arthur, M. A., Dean, W. E., and Schlanger, S. O. (1985). "Variations in the global carbon cycle during the Cretaceous related to climate, volcanism, and changes in atmospheric CO_2," in *The carbon cycle and atmospheric CO2: Natural variations archean to present. Geophysical monograph*. Editors E. T. Sundquist and W. S. Broecker (Hoboken, N J, USA: Wiley-Blackwell), 504–529.

Azmy, K., Brand, U., Sylvester, P., Gleeson, S. A., Logan, A., and Bitner, M. A. (2011). Biogenic and abiogenic low-Mg calcite (bLMC and aLMC): Evaluation of seawater-REE composition, water masses and carbonate diagenesis. *Chem. Geol.* 280 (1-2), 180–190. doi:10.1016/j.chemgeo.2010.11.007

Baud, A., Magaritz, M., and Holser, W. T. (1989). Permian-triassic of the tethys: Carbon isotope studies. *Geol. Rundsch.* 78 (2), 649–677. doi:10.1007/bf01776196

Bond, D. P. G., Wignall, P. B., Wang, W., Izon, G., Jiang, H. S., Lai, X. L., et al. (2010). The mid-Capitanian (Middle Permian) mass extinction and carbon isotope record of South China. *Palaeogeogr. Palaeoclimatol. Palaeoecol.* 292, 282–294. doi:10.1016/j.palaeo.2010.03.056

Burgess, S. D., and Bowring, S. A. (2015). High-precision geochronology confirms voluminous magmatism before, during, and after Earth's most severe extinction. *Sci. Adv.* 1, e1500470. doi:10.1126/sciadv.1500470

Cao, C. Q., Cui, C., Chen, J., Summons, R. E., Shen, S. Z., and Zhang, H. (2018). A positive C-isotope excursion induced by sea-level fall in the middle Capitanian of South China. *Palaeogeogr. Palaeoclimatol. Palaeoecol.* 505, 305–316.doi:10.1016/j.palaeo.2018.06.010

Chen, B., Chen, J. T., Qie, W. K., Huang, P., He, T. C., Joachimski, M. M., et al. (2021). Was climatic cooling during the earliest Carboniferous driven by expansion of seed plants. *Earth Planet. Sci. Lett.* 565, 116953.doi:10.1016/j.epsl.2021.116953

Chen, B., Joachimski, M. M., Sun, Y. D., Shen, S. Z., and Lai, X. L. (2011). Carbon and conodont apatite oxygen isotope records of Guadalupian-Lopingian boundary sections: Climatic or sea-level signal? *Palaeogeogr. Palaeoclimatol. Palaeoecol.* 311 (3-4), 145–153. doi:10.1016/j.palaeo.2011.08.016

Chen, J. T., Montañez, I. P., Qi, Y. P., Shen, S. Z., and Wang, X. D. (2018). Strontium and carbon isotopic evidence for decoupling of pCO_2 from continental weathering at the apex of the late Paleozoic glaciation. *Geology* 46, 395–398. doi:10.1130/g40093.1

Chen, J. T., Montañez, I. P., Zhang, S., Isson, T. T., Macarewich, S. I., Planavsky, N. J., et al. (2022). Marine anoxia linked to abrupt global warming during Earth's penultimate icehouse. *Proc. Natl. Acad. Sci. U. S. A.* 119 (19), e2115231119. doi:10.1073/pnas.2115231119

Chen, J., and Xu, Y. G. (2019). Establishing the link between permian volcanism and biodiversity changes: Insights from geochemical proxies. *Gondwana Res.* 75, 68–96. doi:10.1016/j.gr.2019.04.008

Chen, Z. Q., George, A. D., and Yang, W-R. (2009). Effects of Middle-Late Permian sea-level changes and mass extinction on the formation of the Tieqiao skeletal mound in the Laibin area, South China. *Aust. J. Earth Sci.* 56, 745–763. doi:10.1080/08120090903002581

Cochran, J. K., Kallenberg, K., Landman, N. H., Harries, P. J., Weinreb, D., Turekian, K. K., et al. (2010). Effect of diagenesis on the Sr, O, and C isotope composition of late cretaceous mollusks from the western interior seaway of north America. *Am. J. Sci.* 310, 69–88. doi:10.2475/02.2010.01

Courtillot, V. E., and Renne, P. R. (2003). On the ages of flood basalt events. *Comptes Rendus Geosci.* 335 (1), 113–140. doi:10.1016/s1631-0713(03)00006-3

Courtillot, V. (1999). *Evolutionary catastrophes: The science of mass extinction*. New York, USA: Cambridge University Press.

Davydov, V. I. (2014). Warm water benthic foraminifera document the Pennsylvanian–Permian warming and cooling events-The record from the Western Pangea tropical shelves. *Palaeogeogr. Palaeoclimatol. Palaeoecol.*, 284–295.414.doi:10.1016/j.palaeo.2014.09.013

Davydov, V. I., Budnikov, I. V., Kutygin, R. V., Nurgalieva, N. G., Biakov, A. S., Karasev, E. V., et al. (2022). Possible bipolar global expression of the P3 and P4 glacial events of eastern Australia in the Northern Hemisphere: Marine diamictites and glendonites from the middle to upper Permian in southern Verkhoyanie, Siberia. *Geology* (8), 874–879.50.doi:10.1130/G50165.1

Day, M. O., Ramezani, J., Bowring, S. A., Sadler, P. M., Erwin, D. H., Abdala, F., et al. (2015). When and how did the terrestrial mid-permian mass extinction occur? Evidence from the tetrapod record of the karoo basin, south Africa. *Proc. R. Soc. B* 282, 20150834–20150838. doi:10.1098/rspb.2015.0834

Denison, R. E., Koepnick, R. B., Burke, W. H., Hetherington, E. A., and Fletcher, A. (1994). Construction of the mississippian, pennsylvanian and permian seawater 87Sr/86Sr curve. *Chem. Geol.* 112, 145–167. doi:10.1016/0009-2541(94)90111-2

Derry, L. A., Kaufman, A. J., and Jacobsen, S. B. (1992). Sedimentary cycling and environmental change in the Late Proterozoic: Evidence from stable and radiogenic isotopes. *Geochimica Cosmochimica Acta* 56 (3), 1317–1329. doi:10.1016/0016-7037(92)90064-p

Dong, Y. X., Xu, S. L., Wen, L., Chen, H. D., Fu, S. Y., Zhong, Y. J., et al. (2020). Tectonic control of guadalupian-lopingian cherts in northwestern sichuan basin, south China. *Palaeogeogr. Palaeoclimatol. Palaeoecol.* 557, 109915. doi:10.1016/j.palaeo.2020.109915

Fan, J. X., Shen, S. Z., Erwin, D. H., Sadler, P. M., MacLeod, N., Cheng, Q. M., et al. (2020). A high-resolution summary of Cambrian to Early Triassic marine invertebrate biodiversity. *Science* 367, 272–277. doi:10.1126/science.aax4953

Foster, G. L., Royer, D. L., and Lunt, D. J. (2017). Future climate forcing potentially without precedent in the last 420 million years. *Nat. Commun.* 8, 14845. doi:10.1038/ncomms14845

Frank, T. D., Shultis, A. I., and Fielding, C. R. (2015). Acme and demise of the late palaeozoic ice age: A view from the southeastern margin of gondwana. *Palaeogeogr. Palaeoclimatol. Palaeoecol.* 418, 176–192. doi:10.1016/j.palaeo.2014.11.016

Groves, J. R., and Wang, Y. (2013). Timing and size selectivity of the Guadalupian (Middle Permian) fusulinoidean extinction. *J. Paleontol.* 87, 183–196. doi:10.1666/12-076r.1

Haq, B. U., and Schutter, S. R. (2008). A chronology of Paleozoic sea-level changes. *Science* 322, 64–68. doi:10.1126/science.1161648

He, B., Xu, Y. G., Chung, S. L., Xiao, L., and Wang, Y. M. (2003). Sedimentary evidence for a rapid, kilometer-scale crustal doming prior to the eruption of the Emeishan flood basalts, *Earth and Planetary Sciences Letters*, doi:10.1016/S0012-821X(03)00323-6213, 391–405.

Hou, Z. S., Fan, J. X., Henderson, C. M., Yuan, D. X., Shen, B. H., Wu, J., et al. (2020). Dynamic palaeogeographic reconstructions of the wuchiapingian stage (lopingian, late permian) for the South China block. *Palaeogeogr. Palaeoclimatol. Palaeoecol.* 546, 109667. doi:10.1016/j.palaeo.2020.109667

Hu, S. Z. (2000). *New consideration of gufong formation by stratigraphy check up* 21 (01), 63–68. Nanjing, China: Volcanology & Mineral Resources.

Huang, H., Cawood, P. A., Hou, M. C., Ni, S. J., Yang, J. H., Du, Y. S., et al. (2018). Provenance of late Permian volcanic ash beds in South China: Implications for the age of Emeishan volcanism and its linkage to climate cooling. *Lithos* 314-315, 293–306. doi:10.1016/j.lithos.2018.06.009

Huang, H., Hou, M. C., Qing, H. R., Zhou, L., Yang, J. H., Du, Y. S., et al. (2019b). The contribution of the Emeishan large igneous province to the strontium isotope evolution of the Capitanian seawater. *Int. Geol. Rev.* 61 (15), 1927–1939. doi:10.1080/00206814.2019.1571448

Huang, H., Huyskens, M. H., Yin, Q. Z., Cowood, P. A., Hou, M. C., Yang, J. H., et al. (2022). *Geology.*Eruptive tempo of Emeishan large igneous province, southwestern China and northern Vietnam: Relations to biotic crises and paleoclimate changes around the Guadalupian-Lopingian boundary, 50, 1083-1087, doi:10.1130/G50183.1

Huang, S. J. (1994). Carbon isotopic of Permian and Permian-Triassic boundary in Upper Yangtze platform and the mass extinction. *Geochimica* 23 (01), 60–68. doi:10.19700/j.0379-1726.1994.01.007

Huang, Y. G., Chen, Z. Q., Wignall, P. B., Grasby, S. E., Zhao, L. S., Wang, X. D., et al. (2019a). Biotic responses to volatile volcanism and environmental stresses over the Guadalupian-Lopingian (Permian) transition. *Geology* 47, 175–178.doi:10.1130/G45283.1

Isozaki, Y., Aljinovic, D., and Kawahata, H. (2011). The guadalupian (permian) Kamura event in European tethys. *Palaeogeogr. Palaeoclimatol. Palaeoecol.* 308, 12–21. doi:10.1016/j.palaeo.2010.09.034

Isozaki, Y. (2009). Illawarra Reversal: The fingerprint of a superplume that triggered Pangean breakup and the end-Guadalupian (Permian) mass extinction. *Gondwana Res.* 15, 421–432. doi:10.1016/j.gr.2008.12.007

Isozaki, Y., Kawahata, H., and Minoshima, K. (2007). The capitanian (permian) Kamura cooling event: The beginning of the paleozoic-mesozoic transition. *Palaeoworld* 16, 16–30. doi:10.1016/j.palwor.2007.05.011

Isozaki, Y. (1997). Permo-triassic boundary superanoxia and stratified superocean: Records from lost deep sea. *Science* 276, 235–238. doi:10.1126/science.276.5310.235

Isson, T. T., Planavsky, N. J., Coogan, L. A., Stewart, E. M., Ague, J. J., Bolton, E. W., et al. (2019). Evolution of the global carbon cycle and climate regulation on Earth. *Glob. Biogeochem. Cycles* 34, e2018GB006061. doi:10.1029/2018gb006061

Jin, Y. G., Wang, W., Wang, Y., and Cao, C. Q. (1998). "Prospects for global correlation of Permian sequences,". Editors G. R. Shi, N. W. Archbold, and M. Grover (Proc. Roy. Soc. Victoria), 10, 73–83.*Strzelecki Int. Symposium Permian East. Tethys Biostratigr. Palaeogeogr. Resour*.doi:10.1016/S0920-5446(00)80006-0

Jin, Y. G., Zhang, J., and Shang, Q. H. (1994). "Two phases of the end-Permian mass extinction," in *Canadian society of Petroleum geologists, memoir 17*. Editors A. F. Embry, B. Beauchamp, and D. J. Glass (Calgary: Can. Soc. Petrol. Geol), 813–822.

Jost, A. B., Mundil, R., He, B., Brown, S. T., Altiner, D., Sun, Y. D., et al. (2014). Constraining the cause of the end-Guadalupian extinction with coupled records of carbon and calcium isotopes. *Earth And Planet. Sci. Lett.* 396, 201–212. doi:10.1016/j.epsl.2014.04.014

Kani, T., Hisanabe, C., and Isozaki, Y. (2013). The Capitanian (Permian) minimum of 87Sr/86Sr ratio in the mid-Panthalassan paleo-atoll carbonates and its demise by the deglaciation and continental doming. *Gondwana Res.* 24 (1), 212–221. doi:10.1016/j.gr.2012.08.025

Kaufman, A. J., and Knoll, A. H. (1995). Neoproterozoic variations in the C-isotopic composition of seawater: Stratigraphic and biogeochemical implications. *Precambrian Res.* 73 (1-4), 27–49. doi:10.1016/0301-9268(94)00070-8

Knauth, L. P., and Kennedy, M. J. (2009). The late Precambrian greening of the Earth. *Nature* 460, 728–732. doi:10.1038/nature08213

Korte, C., Jasper, T., Kozur, H. W., and Veizer, J. (2006). 87Sr/86Sr record of Permian seawater. *Palaeogeogr. Palaeoclimatol. Palaeoecol.* 240, 89–107. doi:10.1016/j.palaeo.2006.03.047

Korte, C., and Kozur, H. W. (2010). Carbon-isotope stratigraphy across the permian-triassic boundary: A review. *J. Asian Earth Sci.* 39, 215–235. doi:10.1016/j.jseaes.2010.01.005

Kump, L. R., and Arthur, M. A. (1999). Interpreting carbon-isotope excursions: Carbonates and organic matter. *Chem. Geol.* 161, 181–198. doi:10.1016/s0009-2541(99)00086-8

Lai, X. L., Wang, W., Wignall, P. B., Bond, D. P. G., Jiang, H. S., Ali, J. R., et al. (2008). Palaeoenvironmental change during the end-Guadalupian (Permian) mass extinction in Sichuan, China. *Palaeogeogr. Palaeoclimatol. Palaeoecol.* 269, 78–93. doi:10.1016/j.palaeo.2008.08.005

Li, D. D., Zhang, X. L., Hu, D. P., Chen, X. Y., Huang, W., Zhang, X., et al. (2018a). Evidence of a large δ13Ccarb and δ13Corg depth gradient for deep-water anoxia during the late Cambrian SPICE event. *Geology* 46 (7), 631–634. doi:10.1130/g40231.1

Li, G. J., and Elderfield, H. (2013). Evolution of carbon cycle over the past 100 million years. *Geochimica Cosmochimica Acta* 103, 11–25. doi:10.1016/j.gca.2012.10.014

Li, Q., Yang, S., Azmy, K., Chen, H. D., Hou, M. C., Wang, Z. J., et al. (2021). Strontium isotope evolution of middle permian seawater in the sichuan basin, south China: Possible causes and implications. *Palaeogeogr. Palaeoclimatol. Palaeoecol.* 565, 110188. doi:10.1016/j.palaeo.2020.110188

Li, W. P., Zheng, Y. F., and Zhao, Y. Y. (2017). Geochemical evidence from marine carbonate for enhanced terrigenous input into seawater during the Ediacaran-Cambrian transition in South China. *Precambrian Res.* 291, 83–97. doi:10.1016/j.precamres.2017.01.015

Li, X. N. (2016). *Stable carbon and oxygen isotope composition of marine carbonate rocks of the lower triassic in sichuan and chongqing areas*. Chengdu, China: Chengdu University of Technology, 1–161.

Li, Y., He, H., Ivanov, A. V., Demonterova, E. I., Pan, Y., Deng, C., et al. (2018b). 40Ar/39Ar age of the onset of high-Ti phase of the Emeishan volcanism strengthens the link with the end-Guadalupian mass extinction. *Int. Geol. Rev.* (15), 1–12.60.doi:10.1080/00206814.2017.1405748

Liu, X. C., Wang, W., Shen, S. Z., Gorgij, M. N., Ye, F. C., Zhang, Y. C., et al. (2013). Late Guadalupian to Lopingian (Permian) carbon and strontium isotopic chemostratigraphy in the Abadeh section, central Iran. *Gondwana Res.* 24, 222–232. doi:10.1016/j.gr.2012.10.012

Macdonald, F. A., Swanson-Hysell, N. l., Park, Y., Lisiecki, L., and Jagoutz, O. (2019). Arc-continent collisions in the tropics set Earth's climate state. *Science* 364, 181–184. doi:10.1126/science.aav5300

Maruyama, S., Santosh, M., and Zhao, D. P. (2007). Superplume, supercontinent, and postperovskite: Mantle dynamics and anti-plate tectonics on the core-mantle boundary. *Gondwana Res.* 11, 7–37. doi:10.1016/j.gr.2006.06.003

McArthur, J. M., Howarth, R. J., and Shields, G. A. (2012). "Strotium isotope stratigraphy," in *The geological time scale 2012*. Editors F. M. Gradstein, J. G. Ogg, M. D. Schmitz, and G. M. Ogg (Amsterdam: Elsevier), 127–144.

McArthur, J. M., Howarth, R. J., Shields, G. A., and Zhou, Y. (2020). "Strontium isotope stratigraphy, Chapter 7," in *Geologic time scale 2020*. Editors F. M. Gradstein, J. G. Ogg, M. D. Schmitz, and G. M. Ogg (Elsevier), 211–238.Amsterdam.

McArthur, J. M., and Howarth, R. J. (2004). Strontium isotope stratigraphy. *Geol. Time Scale 2012* 1, 127–144.doi:10.1016/B978-0-12-824360-2.00007-3

Mei, S. L., Jin, Y. G., and Wardlaw, B. R. (1994a). Succession of conodont zones from the permian "kuhfeng" formation, xuanhan, sichuan and its implications in global correlation. *Acta Palaeontol. Sin.* 33, 1–23. (in Chinese with English abstract).

Mei, S. L., Jin, Y. G., and Wardlaw, B. R. (1994b). Sucession of Wuchiapingian conodonts from northeastern Sichuan and its worldwide correlation. *Acta Micropalaeontol Sin.* 11, 121–139.

Mei, S. L. (1995). The best natural boundary: A new concepet for stratigraphic division developed by combining the sequence boundary with the gssp. *Acta Geol. Sin.* (03), 277–284.

Metcalfe, I., Crowley, J. L., Nicoll, R. S., and Schmitz, M. (2015). High-precision U-Pb CA-TIMS calibration of Middle Permian to Lower Triassic sequences, mass extinction and extreme climate-change in eastern Australian Gondwana. *Gondwana Res.* 28, 61–81. doi:10.1016/j.gr.2014.09.002

Murchey, B. L., and Jones, D. L. (1992). A mid-permian chert event: Widespread deposition of biogenic siliceous sediments in coastal, island arc and oceanic basins. *Palaeogeogr. Palaeoclimatol. Palaeoecol.* 96, 161–174. doi:10.1016/0031-0182(92)90066-e

Nier, A. O. (1938). The isotopic constitution of strontium, barium, bismuth, thallium and mercury. *Phys. Rev.* 54 (4), 275–278. doi:10.1103/physrev.54.275

Peucker-Ehrenbrink, B., and Fiske, G. J. (2019). A continental perspective of the seawater 87Sr/86Sr record: A review. *Chem. Geol.* 510, 140–165. doi:10.1016/j.chemgeo.2019.01.017

Qiu, W. T., and Gu, H. X. (1991). Sedimentary environments of the chert (siliceous rocks) from the lower Permian Gufeng formation in northeastern Sichuan. *Acta Palaeontol. Sin.* 01, 001.

Qiu, Z., and Wang, Q. (2011). Geochemical evidence for submarine hydrothermal origin of the Middle-Upper Permian chert in Laibin of Guangxi, China. *Sci. China Earth Sci.* 54, 1011–1023. doi:10.1007/s11430-011-4198-x

Rimmer, S. M. (2004). Geochemical paleoredox indicators in devonian-mississippian black shales, central appalachian basin (USA). *Chem. Geol.* 206, 373–391. doi:10.1016/j.chemgeo.2003.12.029

Ross, C. A., and Ross, J. R. P. (1987). "Late Paleozoic sea levels and depositional sequences,". Editors C. A. Ross and D. Haman (Cushman Foundation for Foraminiferal Research: Special Publication), 24, 137–149.*Timing Depositional Hist. Eustatic Sequences Constraints Seismic Stratigr.*

Saltzman, M. R., Ripperdan, R. L., Brasier, M. D., Lohmann, K. C., Robison, R. A., Chang, W. T., et al. (2000). A global carbon isotope excursion (SPICE) during the late cambrian: Relation to trilobite extinctions, organic-matter burial and sea level. *Palaeogeogr. Palaeoclimatol. Palaeoecol.* 162, 211–223. doi:10.1016/s0031-0182(00)00128-0

Saltzman, M. R., and Thomas, E. (2012). "Carbon isotope stratigraphy," in *The geologic time scale 2012*. F. M. Gradstein, J. G. Ogg, M. Schmitz, et al. (Amsterdam: Elsevier), 207–232.

Santosh, M., Maruyama, S., and Yamamoto, S. (2009). The making and breaking of supercontinents: Some speculations based on superplumes, super downwelling and the role of tectosphere. *Gondwana Res.* 15, 324–341. doi:10.1016/j.gr.2008.11.004

Schoepfer, S. D., Shen, J., Wei, H., Tyson, R. V., Ingall, E., and Algeo, T. J. (2015). Total organic carbon, organic phosphorus, and biogenic barium fluxes as proxies for paleomarine productivity. *Earth. Sci. Rev.* 149, 23–52. doi:10.1016/j.earscirev.2014.08.017

Scholz, F., Hensen, C., Noffke, A., Rohde, A., Liebetrau, V., and Wallmann, K. (2011). Early diagenesis of redox-sensitive trace metals in the Peru upwelling area-response to ENSO-related oxygen fluctuations in the water column. *Geochimica Cosmochimica Acta.*, 7257–7276.75

Scotese, C. R. (2016). *PALEOMAP PaleoAtlas for GPlates and the PaleoData plotter Program*.

Shellnutt, J. G., Denyszyn, S. W., and Mundil, R. (2012). Precise age determination of mafic and felsic intrusive rocks from the Permian Emeishan large igneous province (SW China). *Gondwana Res.* 22 (1), 118–126. doi:10.1016/j.gr.2011.10.009

Shellnutt, J. G., Pham, T. T., Denyszyn, S. W., Yeh, M. W., and Tran, T. A. (2020). Magmatic duration of the Emeishan large igneous province: Insight from northern Vietnam. *Geology* 48 (5), 457–461. doi:10.1130/g47076.1

Shellnutt, J. G. (2014). The emeishan large igneous province: A synthesis. *Geosci. Front.* 5, 369–394. doi:10.1016/j.gsf.2013.07.003

Shembilu, N. C., and Azmy, K. (2022). Trace element variations across Middle-Upper Cambrian carbonates: Implications for the paleoenvironment of eastern Laurentia. *Mar. Petroleum Geol.* 135, 105385. ISSN 0264-8172. doi:10.1016/j.marpetgeo.2021.105385

Shen, J., Schoepfer, S. D., Feng, Q. L., Zhou, L., Yu, J. X., Song, H. Y., et al. (2014). Marine productivity changes during the end-Permian crisis and Early Triassic recovery. *Earth-Science Rev.* 149, 136–162. doi:10.1016/j.earscirev.2014.11.002

Shen, S., Crowley, J. L., Wang, Y., Bowring, S. A., Erwin, D. H., Sadler, P. M., et al. (2011). Calibrating the end-Permian mass extinction. *Science* 334, 1367–1372. doi:10.1126/science.1213454

Shen, S. Z., Cao, C. Q., Zhang, H., Bowring, S. A., Henderson, C. M., Payne, J. L., et al. (2013). High-resolution δ13Ccarb chemostratigraphy from latest guadalupian through earliest triassic in South China and Iran. *Earth And Planet. Sci. Lett.* 375, 156–165. doi:10.1016/j.epsl.2013.05.020

Shen, S. Z., Ramezani, J., Chen, J., Cao, C. Q., Erwin, D. H., Zhang, H., et al. (2019). A sudden end-Permian mass extinction in South China. *GSA Bull.* 131, 205–223. doi:10.1130/b31909.1

Shen, S. Z., and Shi, G. R. (1996). Diversity and extinction patterns of permian brachiopoda of South China. *Hist. Biol.* 12, 93–110. doi:10.1080/08912969609386558

Shen, S. Z., and Shi, G. R. (2002). Paleobiogeographical extinction patterns of permianbrachiopods in the asian-Western pacific region. *Paleobiology* 28, 449–463. doi:10.1666/0094-8373(2002)028<0449:pepopb>2.0.co;2

Shen, S. Z., Yuan, D. X., Henderson, C. M., Lambert, L. L., Zhang, Y. C., Erwin, D. H., et al. (2022). *The global stratotype section and point (GSSP) for the base of the capitanian stage (guadalupian, middle permian)* 45 (3). Nanjing, China: Episodes. doi:10.18814/epiiugs/2022/022004

Shen, S. Z., Yuan, D. X., Henderson, C. M., Wu, Q., Zhang, Y. C., Zhang, H., et al. (2020). Progress, problems and prospects: An overview of the guadalupian series of South China and north America. *Earth-Science Rev.* 221, 103412. doi:10.1016/j.earscirev.2020.103412

Stanley, S. M. (2016). Estimates of the magnitudes of major marine mass extinctions in Earth history. *Proc. Natl. Acad. Sci. U. S. A.* 113, E6325-E6334–E6334. doi:10.1073/pnas.1613094113

Stanley, S. M., and Yang, X. (1994). A double mass extinction at the end of the Paleozoic Era. *Science* 266, 1340–1344. doi:10.1126/science.266.5189.1340

Sun, S., Chen, A. Q., Hou, M. C., Yang, S., Ogg, J. G., Zou, H., et al. (2022). Rapid climatic fluctuations during the Guadalupian-Lopingian transition: Implications from weathering indices recorded in acid-insoluble residues of carbonate rocks, South China. *J. Asian Earth Sci.* 230, 105222. doi:10.1016/j.jseaes.2022.105222

Sun, Y. D., Lai, X. L., Wignall, P. B., Widdowson, M., Ali, J. R., Jiang, H. S., et al. (2010). Dating the onset and nature of the Middle Permian Emeishan large igneous province eruptions in SW China using conodont biostratigraphy and its bearing on mantle plume uplift models. *Lithos* 119, 20–33. doi:10.1016/j.lithos.2010.05.012

Svensen, H., Planke, S., Chevallier, L., Malthe-Sorenssen, A., Corfu, F., and Jamtveit, B. (2007). Hydrothermal venting of greenhouse gases triggering Early Jurassic global warming. *Earth Planet. Sci. Lett.* 256, 554–566. doi:10.1016/j.epsl.2007.02.013

Svensen, H., Planke, S., Polozov, A. G., Schmidbauer, N., Corfu, F., Podladchikov, Y. Y., et al. (2009). Siberian gas venting and the end-Permian environmental crisis. *Earth Planet. Sci. Lett.* 277, 490–500. doi:10.1016/j.epsl.2008.11.015

Takahashi, S., Ogawa, Y., Yamasaki, S. I., Ogawa, Y., Kimura, K., Kaiho, K., et al. (2014). Bioessential element-depleted ocean following the euxinic maximum of the end-Permian mass extinction. *Earth Planet. Sci. Lett.* 393, 94–104. doi:10.1016/j.epsl.2014.02.041

Tierney, K. E. (2010). *Carbon and strontium isotope stratigraphy of the permian from Nevada and China: Implications from an icehouse to greenhouse transition*. Columbus, ProQuest Dissertations and Theses Global: The Ohio State University.

Tribovillard, N., Algeo, T., Lyons, T., and Riboulleau, A. (2006). Trace metals as paleoredox and paleoproductivity proxies: An update. *Chem. Geol.* 232 (1-2), 12–32. doi:10.1016/j.chemgeo.2006.02.012

Veizer, J., Ala, D., Azmy, K., Bruckschen, P., Buhl, D., Bruhn, F., et al. (1999). 87Sr/86Sr, δ13C and δ18O evolution of Phanerozoic seawater. *Chem. Geol.* 161, 59–88. doi:10.1016/s0009-2541(99)00081-9

Veizer, J. (1983). Chemical diagenesis of carbonates: Theory and application. *Stable isotopes Sediment. Geol.* 10, 3–100.

Wang, W. Q., Garbelli, C., Zheng, Q. F., Chen, J., Liu, X. C., Wang, W., et al. (2018). Permian 87Sr/86Sr chemostratigraphy from carbonate sequences in South China. *Palaeogeogr. Palaeoclimatol. Palaeoecol.* 500, 84–94. doi:10.1016/j.palaeo.2018.03.035

Wang, W. Q., Katchinoff, J. A. R., Garbelli, G., Immenhauser, A., Zheng, Q. F., Zhang, Y. C., et al. (2021). Revisiting the Permian seawater 87Sr/86Sr record: New perspectives from brachiopod proxy data and stochastic oceanic box models. *Earth-Science Rev.* 218, 103679. doi:10.1016/j.earscirev.2021.103679

Wang, W. Q., Zhang, F. F., Shen, S. Z., Bizzarro, M., Garbelli, C., Zheng, Q. F., et al. (2022). Constraining marine anoxia under the extremely oxygenated Permian atmosphere using uranium isotopes in calcitic brachiopods and marine carbonates. *Earth Planet. Sci. Lett.* (220), 117714.594

Wang, X. D., and Sugiyama, T. (2000). Diversity and extinction patterns of Permian coral faunas of China. *Lethaia* 33, 285–294. doi:10.1080/00241160750053853

Wang, X. T., Shao, L. Y., Eriksson, K. A., Yan, Z. M., Wang, J. M., Li, H., et al. (2020). Evolution of a plume-influenced source-to-sink system: An example from the coupled Central Emeishan large igneous province and adjacent Western Yangtze cratonic basin in the Late Permian, SW China. *Earth-Science Rev.* 207, 103224. doi:10.1016/j.earscirev.2020.103224

Wedepohl, K. H. (1971). "Environmental influences on the chemical composition of shales and clays," in *Physics and chemistry of the Earth*. Editors L. H. Ahrens, F. Press, S. K. Runcorn, and H. C. Urey (Oxford: Pergamon), 305–333.

Wedepohl, K. H. (1991). "The composition of the upper Earth's crust and the natural cycles of selected metals," in *Metals and their compounds in the environment*. Editor E. Merian (Weinheim: VCH-Verlagsgesellschaft), 3–17.

Wei, H. Y., Tang, Z. W., Yan, D. T., Wang, J. G., and Roberts, A. P. (2019). Guadalupian (Middle Permian) ocean redox evolution in South China and its implications for mass extinction. *Chem. Geol.* 530, 119318. doi:10.1016/j.chemgeo.2019.119318

Wei, H. Y., Wei, X. M., Qiu, Z., Song, H. Y., and Shi, G. (2016). Redox conditions across the G-L boundary in South China: Evidence from pyrite morphology and sulfur isotopic compositions. *Chem. Geol.* 440, 1–14. doi:10.1016/j.chemgeo.2016.07.009

Wignall, P. B. (2001). Large igneous provinces and mass extinctions. *Earth-Science Rev.* 53, 1–33. doi:10.1016/s0012-8252(00)00037-4

Wignall, P. B., Sun, Y. D., Bond, D. P. G., Izon, G., Newton, R. J., Vedrine, S., et al. (2009). Volcanism, mass extinction, and carbon isotope fluctuations in the Middle Permian of China. *Science* 324, 1179–1182. doi:10.1126/science.1171956

Wignall, P. B., and Twitchett, R. J. (1996). Oceanic anoxia and the end Permian mass extinction. *Science* 272, 1155–1158. doi:10.1126/science.272.5265.1155

Xu, Y. G., Chung, S. L., Shao, H., and He, B. (2010). Silicic magmas from the emeishan large igneous province, southwest China: Petrogenesis and their link with the end-guadalupian biological crisis. *Lithos* 119, 47–60. doi:10.1016/j.lithos.2010.04.013

Yan, D. T., Zhang, L. Q., and Qiu, Z. (2013). *Carbon and sulfur isotopic fluctuations associated with the end-Guadalupian mass extinction in South China*.

Yang, J. H., Cawood, P. A., Du, Y. D., Condon, D. J., Yan, J. X., Liu, J. Z., et al. (2018). Early Wuchiapingian cooling linked to Emeishan basaltic weathering? *Earth Planet. Sci. Lett.* 492, 102–111. doi:10.1016/j.epsl.2018.04.004

Yang, S., Chen, A. Q., Zhang, X. H., Li, Q., Xu, S. L., Chen, C., et al. (2021). Paleogeographic transition of the permian chihsia-maokou period in the sichuan basin and indications for oil-gas exploration. *Acta Sedimentol. Sin.* 39 (06), 1466–1477.

Yao, X., Zhou, Y. Q., and Hinnov, L. A. (2015). Astronomical forcing of a middle permian chert sequence in chaohu, south China. *Earth And Planet. Sci. Lett.* 422, 206–221. doi:10.1016/j.epsl.2015.04.017

Yuan, D. X. (2015). *Comparative study on the guadalupian (middle permian) conodont biostratigraphy and environmental evolution between South China and north America*. Nanjing, China: Nanjing University, 1–148.

Zhang, B. L., Wignall, P. B., Yao, S. P., Hu, W. X., and Liu, B. (2021a). Collapsed upwelling and intensified euxinia in response to climate warming during the Capitanian (Middle Permian) mass extinction. *Gondwana Res.*, 31–46.89.

Zhang, H., Zhang, F. F., Chen, J. B., Erwin, D. H., Syverson, D. D., Ni, P., et al. (2021b). Felsic volcanism as a factor driving the end-Permian mass extinction. *Sci. Adv.* 7(47: eabh1390.

Zhao, Z. F., Thibault, N., Dahl, T. W., Schovsbo, N. H., Sørensen, A. L., Rasmussen, C. M. Ø., et al. (2022). Synchronizing rock clocks in the late Cambrian. *Nat. Commun.* 13, 1990.

Zhong, Y., Mundil, R., Chen, J., Yuan, D., Denyszyn, S. W., Jost, A. B., et al. (2020). Geochemical, biostratigraphic, and high-resolution geochronological constraints on the waning stage of Emeishan Large Igneous Province. *GSA Bull.* 132 (9-10), 1969–1986. doi:10.1130/b35464.1

Zhong, Y. T., He, B., Mundil, R., and Xu, Y. G. (2014). CA-TIMS zircon U-Pb dating of felsic ignimbrite from the Binchuan section: Implications for the termination age of Emeishan large igneous province. *Lithos* 204, 14–19. doi:10.1016/j.lithos.2014.03.005